

**Synthesis and Characterization of Amylopectin-grafted
Polyacrylamide (AP-*g*-PAM) Flocculants for Dewatering of
Oil Sands Mature Fine Tailings (MFT)**

by

Behnaz Bazoubandi

A thesis submitted in partial fulfillment of the requirements for the degree of

Master of Science

in

Chemical Engineering

**Department of Chemical and Materials Engineering
University of Alberta**

Abstract

Oil sand mining continues increasing in Alberta and bitumen production from surface mining is predicted to reach 257,600 m³/day by 2026 (a 41.3% increase compared to 2016), generating a large amount of tailings that need to be stored in tailing ponds. The challenging part of tailing management is to dewater mature fine tailings (MFT), as the fine solids dispersed in MFT are not easily separated from water by gravity. A possible way to conquer this challenge is to use polymer flocculants to dewater MFT.

This research evaluates the performance of amylopectin-graft-polyacrylamide (AP-g-PAM) to flocculate and dewater MFT. Polyacrylamide was grafted on the amylopectin backbone by free radical polymerization using ceric ammonium nitrate (CAN) as an initiator. AP-g-PAM samples were studied by Fourier transform infrared spectroscopy (FTIR), nuclear magnetic resonance spectroscopy (NMR), thermogravimetric analysis (TGA), and scanning electron microscopy (SEM).

Different grades of AP-g-PAM were synthesized and tested to flocculate MFT. The flocculation performances of the graft polymers were compared with those of commercial polymers based on the supernatant turbidity, sediment solids content, and capillary suction time (CST). Compared to PAM, it was shown that AP-g-PAM was able to form flocs with higher solids content.

Acknowledgements

I am so blessed that I had the opportunity to continue my studies at University of Alberta as a Master's student. Now that this chapter of my life is coming to the end, I would like to express my sincere gratitude to those who helped me make it happen:

Eternal gratitude to my wonderful supervisor, Professor João B. P. Soares: Thank you for being such a kind and well-mannered advisor. I truly appreciate what you did for me; your time dedicated to our weekly meetings, your guidance and support in my research, your precision in reviewing my drafts, and your understanding and patience whenever I had tough times either in my research or personal life. It has been a great privilege for me to be part of your research group. I would also like to thank your kind-hearted wife, Maria, for being always very friendly and nice to me.

Special thanks to Artin Afacan: Thank you very much for helping me in my research project. I learned a lot from you and really appreciate your willingness to help. Thanks for your support and words of encouragement.

Grateful acknowledgement to my exam committee members: Prof. Robert E. Hayes, Prof. Phillip Y. K. Choi, and Prof. Qi Liu.

I am grateful to all the staff at Department of Chemical and Materials Engineering who provide assistant to graduate students with kindness and compassion, especially Lily Laser and Marion Pritchard. Thanks to staff of “nanoFAB Fabrication and Characterization Centre” and “Oil Sands and Coal Interfacial Engineering Facility” who helped me with my characterization tests, especially Ni Yang.

I would like to thank Campus Alberta Innovates Program (CAIP) for providing my research funding.

Thanks to everyone in our research group for making a positive work environment in which everyone could grow. A very special thank you to Dr. Saeid Mehdiabadi, Dr. Marco Antonio da Silva, Dr. Diógenes Vedoy, Sarang Gumfekar, Vahid Vajihinejad, Daniel Moran, and Atreya Nitalla.

To brilliant Dr. Linda Botha: Thank you so much for being such a helpful post-doctoral fellow. You have been always an amazing inspiration and role model for me.

To Zahra Rostami Najafabadi and her husband, Farhad Azam: Thank you for all your help. What you did for me was priceless.

To my best friends, Maryam Akbari, Babak Soltannia, Hassan Teimoori, and Sadra Kayvan: You have been always there for me whenever I needed to be heard. This could have been much more difficult without you. Thank you for letting me count on you.

I am forever indebted to my family for their support and encouragement. To my Dad: Thank you for always believing in me. You are the biggest support in my life and I am very grateful to have an amazing father like you. To my beautiful Mom: You have taught me everything that I know. I am very lucky that a strong woman like you raised me. We cannot thank you enough for what you have done for our family. Thanks to my older sister, Bahar, for being a true friend to me in my entire life who takes care of me better than anyone else. To my little brother, Sina: Thank you for making me laugh even at the toughest times in my life. You are the joy of my life. Thank you for being such an awesome brother.

Behnaz Bazoubandi

Nomenclature

AA	Acrylic acid
AAS	Atomic absorption spectrophotometry
AM	Acrylamide
AP	Amylopectin
AP-g-H-PMA	Amylopectin grafted hydrolyzed poly(methyl acrylate)
AP-g-PAM	Unpurified amylopectin grafted polyacrylamide
AP-PAM	Amylopectin and polyacrylamide blend
ATMAC	(3-acrylamidopropyl) trimethylammonium chloride
CAN	Ceric ammonium nitrate
CHPTAC	N-3-chloro-2-hydroxypropyl trimethyl ammonium chloride
CP ₁	Commercial polyacrylamide from Sigma
CP ₂	Commercial polyacrylamide from Kemira
CST	Capillary suction time
DADMAC	Poly(diallyl dimethyl ammonium chloride)
DMA	N,N-dimethylacrylamide
FFT	Fine fluid tailings
FTIR	Fourier transform infrared spectroscopy
HPMC	Hydroxypropyl methylcellulose
HPMC-g-PAM	Hydroxypropyl methylcellulose grafted polyacrylamide
KPS	Potassium persulfate
MA	Methyl acrylate
MFT	Mature fine tailings
NMR	Nuclear magnetic resonance spectroscopy
NTU	Nephelometric turbidity units
P(AP-g-PAM)	Purified amylopectin grafted polyacrylamide
PAA	Poly acrylic acid
PAM	Polyacrylamide
PATMAC	Poly(3-acrylamidopropyl) trimethylammonium chloride
PDMA	Poly(N,N-dimethylacrylamide)
PEO	Polyethylene oxide
PMA	Poly(methyl acrylate)
PMMA	Poly(methyl methacrylate)
PSD	Particle size distribution
SEM	Scanning electron microscopy
TGA	Thermogravimetric analysis

Different grades of AP-g-PAM were identified by their codes in the “G-#-#” format. The letter “G” stands for graft polymer. The first number following the letter G, is the concentration of AP in the reactor multiplied by 100. The second number in polymer codes, shows the ratio of monomer concentration to initiator concentration divided by 1,000. For instance, G-4-2.5 is a code for a graft polymer that was synthesized with 0.04 mol AGU/L AP and 2,500 monomer to initiator ratio.

Synthesized polyacrylamides were also shown by H-#: The letter “H” stands for homo-polymer and the following number shows the monomer to initiator ratio divided by 1,000. So, the monomer to initiator ratio used in H-2.5 polymerization was 2,500.

Table of Contents

Chapter 1: Introduction	1
1.1. Alberta’s Oil Sands Tailings	1
1.2. Water Purification	5
1.3. Electric Double Layer Forces	7
1.4. Colloid Stability and DLVO Theory	9
1.5. Polymeric Flocculants	12
1.6. Natural, Synthetic, and Graft Polymers	16
1.7. Amylopectin Grafted Flocculants	18
1.8. References	24
Chapter 2: Materials and Methods	30
2.1. General	30
2.2. Experimental	30
2.2.1. Materials	30
2.2.2. Synthesis and Preparation of AP-g-PAM Flocculants	30
2.2.3. Polymer Characterization Tests	35
Fourier Transform Infrared Spectroscopy (FTIR)	35
Nuclear Magnetic Resonance Spectroscopy (NMR)	35
Thermogravimetric Analysis (TGA)	35
Scanning Electron Microscopy (SEM)	36

2.2.4. MFT Characterization Tests	36
Moisture Analysis	36
Dean-Stark Extraction.....	36
Particle Size Distribution (PSD).....	38
Atomic Absorption Spectrophotometry (AAS)	38
2.2.5. Flocculation Tests	39
Jar Test.....	39
Sieve Test.....	41
2.3. References.....	42
Chapter 3: Results and Discussion.....	43
3.1. General.....	43
3.2. AP-g-PAM Characterization.....	43
3.2.1. Fourier Transform Infrared Spectroscopy (FTIR)	43
3.2.2. Nuclear Magnetic Resonance (NMR).....	48
3.2.3. Thermogravimetric Analysis (TGA).....	54
3.2.4. Scanning Electron Microscopy (SEM)	56
3.3. MFT characterization.....	59
Moisture Analysis	59
Dean-Stark Analysis	59
Particle Size Distribution	60
Atomic Absorption Spectrophotometry (AAS)	61
3.4. Flocculation Tests	62

3.4.1. Flocculation Parameters and Reproducibility of Flocculation Tests	62
3.4.2. Amylopectin Flocculation.....	64
3.4.3. AP-g-PAM Flocculation Performance.....	66
3.4.4. Sieve Test.....	74
3.5. References.....	77
Chapter 4: Conclusions and Future Works	79
Bibliography	81
Appendix A: NTU Calibration Curve.....	88
Appendix B: Flocculation Results	91

List of Tables

Table 1.1. Classification of particles according to their sizes.	6
Table 1.2. Amylopectin grafted polymers used as flocculants.	23
Table 2.1. Concentrations of different reagents for the synthesis of AP- <i>g</i> -PAM.	33
Table 2.2. Concentrations of different reagents for the synthesis of PAM.	34
Table 3.1. FTIR samples.	43
Table 3.2. Amylopectin characteristic functional groups and their corresponding FTIR wavenumbers.	46
Table 3.3. Polyacrylamide characteristic functional groups and their corresponding FTIR wavenumbers.	47
Table 3.4. NMR samples.	49
Table 3.5. Amylopectin functional groups and their corresponding ¹ H NMR chemical shifts.	51
Table 3.6. Polyacrylamide functional groups and their corresponding ¹ H NMR chemical shifts.	51
Table 3.7. Amylopectin functional groups and their corresponding ¹³ C NMR chemical shifts.	52

Table 3.8. Polyacrylamide functional groups and their corresponding ¹³ C NMR chemical shifts.	52
Table 3.9. TGA samples.	54
Table 3.10. SEM samples.	57
Table 3.11. Moisture analysis of the MFT.	59
Table 3.12. Dean-Stark analysis of the MFT.	59
Table 3.13. Ion composition of the MFT.	60
Table A.1. Turbidity of MFT solutions with different solid contents.	88
Table B.1. Flocculation Results (Turbidity and Solids Content).	91
Table B.2. Flocculation Results (CSTs of whole suspension and sediment).	93
Table B.3. Sieve tests results at 6,000 ppm.	95
Table B.4. Sieve tests results at 8,000 ppm.	96
Table B.5. Sieve tests results at 10,000 ppm.	97

List of Figures

Figure 1.1. Oil sands deposits in Canada (left) and oil sand structure (right).	1
Figure 1.2. Oil sands tailing pond.	2
Figure 1.3. Electric double layer of a negatively charged particle in aqueous suspension.	8
Figure 1.4. Potential energy of interaction versus distance between two negatively charged particles.	10
Figure 1.5. Possible configurations of a polymer molecule adsorbed onto a surface.	13
Figure 1.6. Polymer bridging mechanism.	13
Figure 1.7. Charge neutralization and charge patch mechanisms.	14
Figure 1.8. Macroscopic schematic for the flocculation process.	15
Figure 1.9. Linear polymer and graft (branched) polymer in a suspension.	17
Figure 1.10. Structure of amylopectin and amylose.	18
Figure 1.11. Schematic of polymerization through grafting-from method.	19
Figure 2.1. Scheme of polymerization set-up.	31
Figure 2.2. Dean-stark apparatus.	38
Figure 3.1. FTIR spectra of AP, PAM, AP-PAM, AP-g-PAM, and P(AP-g-PAM).	45
Figure 3.2. AP and PAM structures.	48
Figure 3.3. Proton NMR chemical shifts for AP, PAM, AP-g-PAM, and AP-PAM.	50

Figure 3.4. Carbon NMR chemical shifts of AP, PAM, AP-g-PAM, and AP-PAM.	53
Figure 3.5. TGA weight loss versus temperature for three different AP-g-PAM samples.	54
Figure 3.6. TGA weight loss versus temperature for AP, PAM, AP-g-PAM, P(AP-g-PAM), and AP-PAM.	56
Figure 3.7. SEM images of AP (left) and AP-g-PAM (right).	57
Figure 3.8. SEM images of AP-PAM, AP, and PAM.	58
Figure 3.9. Particle size distribution (PSD) of the MFT.	60
Figure 3.10. Reproducibility of flocculation and dewatering results.	63
Figure 3.11. Flocculated MFT by AP, H-2.5, AP-H-2.5, and G-4-2.5 after 24 h at different polymer dosages.	65
Figure 3.12. Flocculation results of AP, H-2.5, AP-H-2.5, and G-4-2.5.	66
Figure 3.13. Flocculation performance of G-4-0.25, G-4-2.5, G-4-0.5, and G-4-1.5.	68
Figure 3.14. Flocculation performance of G-4-2.5, G-6-2.5, and G-8-2.5.	70
Figure 3.15. Flocculation performance of G-6-3.5, G-6-2.5, G-8-3.5, and G-8-5.	72
Figure 3.16. Flocculation results of G-6-3.5, CP ₁ , and CP ₂	73
Figure 3.17. Solids content of flocculated MFT for sieve test versus time for CP ₁ , CP ₂ , H-3.5, H-5, G-6-2.5, G-6-3.5, G-8-2.5, G-8-3.5, and G-8-5 at 6,000 ppm.	75
Figure 3.18. Solids content of flocculated MFT for sieve test versus time for CP ₁ , CP ₂ , H-3.5, H-5, G-6-2.5, G-6-3.5, G-8-2.5, G-8-3.5, and G-8-5 at 8,000 ppm.	75

Figure 3.19. Solids content of flocculated MFT for sieve test versus time for CP₁, CP₂, H-3.5, H-5, G-6-2.5, G-6-3.5, G-8-2.5, G-8-3.5, and G-8-5 at 10,000 ppm.....76

Figure A.1. Turbidity calibration curve: Turbidity (NTU) versus solids content (wt. %) of MFT solutions.89

Figure A.2. MFT samples with different solid contents (First number in each picture shows the solid content of MFT suspension (wt. %), and the second one shows the turbidity value in NTU).
.....90

Chapter 1: Introduction

1.1. Alberta's Oil Sands Tailings

Canada has the third largest oil deposits in the world, but differently from conventional crude oil reservoirs, 97 % of the Canadian oil reserves are found in the form of oil sands. Oil sands deposits cover an area of approximately 142,200 km² in the province of Alberta, specifically in Athabasca, Cold Lake, and Peace River regions (Figure 1.1). Only 4,800 km² of these oil sands deposits are shallow enough to be extracted by surface mining [1].

The mined oil sands consist of coarse sand particles, mineral solids, clay, water, electrolytes, and a highly viscous *bitumen* (Figure 1.1). Bitumen needs to be extracted from oil sands and transformed into synthetic crude oil [1-4].

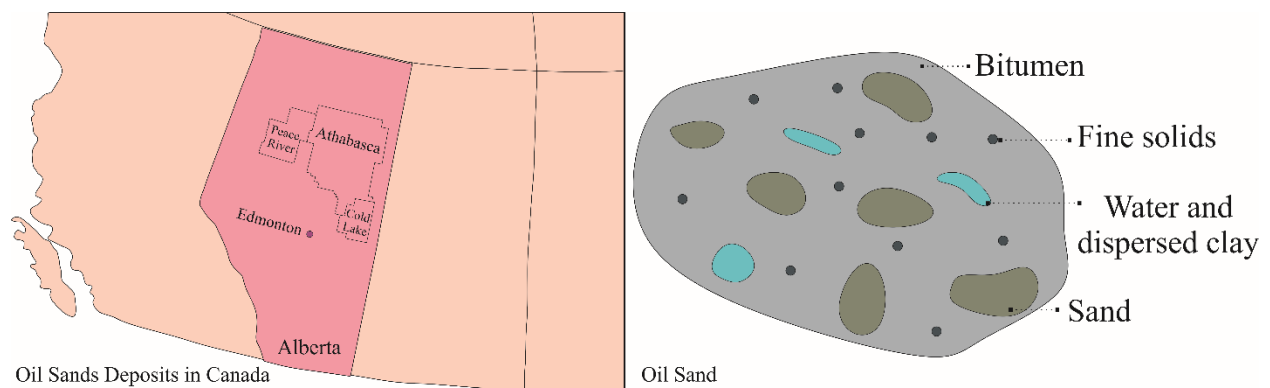


Figure 1.1. Oil sands deposits in Canada (left) and oil sand structure (right) (redrawn from [3,4]).

Normally, 88 to 95 wt. % of the bitumen in oil sands may be extracted using hot water (80-85 °C) and sodium hydroxide (NaOH). The effluent of this process, *oil sands tailings*, contain residual bitumen (less than 5 wt.%), water (approximately 65 wt.%), and solids (approximately 30 wt.%). The solids consist of sand, silt, and negatively charged clay particles (mainly kaolinite and illite). Polycyclic aromatic hydrocarbons, naphthenic acids, heavy metals, and mineral ions may be also found in oil sands tailings. Because these chemicals may be harmful if released into the environment, oil sand tailings are collected temporarily in man-made *tailing ponds* (Figure 1.2) [5].

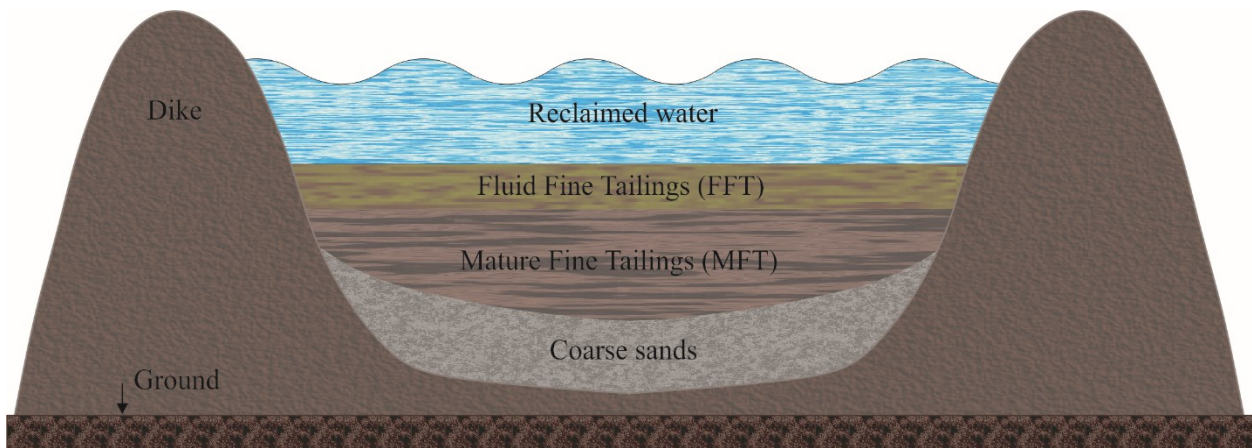


Figure 1.2. Oil sands tailing pond (redrawn from [1]).

The long-term storage of oil sands tailings is bad for the environment. The water in tailings ponds contains toxic compounds that may leak to groundwater and rivers. Birds cannot distinguish between natural lakes and tailings ponds; in 2008, 1600 migrating ducks died in Alberta after landing in a tailing pond and becoming covered with bitumen [6].

Recovery of every barrel of bitumen produces approximately 3.3 m³ tailings, resulting in a daily production of 25 million liters of tailings in Alberta. Today, Alberta's oil sands tailings inventory is more than 1.18 trillion liters, which is more than enough to cover the cities of Toronto and Vancouver. This volume of tailings continues to grow, deepening the negative environmental impact and widening the area occupied land by tailings ponds. Moreover, tailings entrap a large amount of water that cannot be used for decades. Therefore, proper tailing management is essential to recycle the water from oil sands tailings, reclaim the occupied land, and eliminate the environmental impact of the oil sands industry [1,6,7].

Water is reclaimed naturally by gravitational solid-liquid separation in tailings ponds (Figure 1.2). Water is removed from the top of the tailing ponds and transported to bitumen extraction plant, as the solids settle down at the bottom of the pond. Coarse sands settle faster than fine particles, forming the lower part of the sediment bed. The ultrafine particles, with characteristic dimensions smaller than 2 µm, remain suspended for several years, forming the fine fluid tailings (FFT) layer. The fine particles, with characteristic dimensions lower than 44 µm, settle more than the ultrafines, and after few years form a gel-like layer called *mature fine tailings* (MFT). MFT contains approximately 30 to 35 wt.% of solids, which may take several decades to settle by gravity; therefore, dewatering MFT may be the most challenging component of tailings management [2,5,7-9].

The amount of untreated MFT is increasing fast because of the continuous exploration of Canada's oil sands reserves. If this trend continues, the volume of accumulated MFT will reach more than 1 billion cubic meters by 2020. The Alberta Energy Regulator (AER) mandates that oil sands companies recycle the water trapped in MFT and reclaim the land at a rate faster than the production

of oil sands tailings; otherwise, the volume of tailings would increase continuously, with serious negative consequences to Alberta's environment [10].

The properties of the recycled water are also important, because the water must be clean enough to be reused in the bitumen extraction plant. However, reuse of the recycled water is not the only reason for dewatering oil sands tailings, specifically MFT. An equally important goal is to increase the solids content of the sediment at the bottom of the tailing ponds, creating trafficable land ready for reclamation. Oil sands companies must convert the lands being used by tailing ponds to trafficable landscape in 5 years after the tailing deposition is stopped. The strength of the land is normally measured by its ultimate tensile strength, which should be at least 10 kPa for treated tailings ponds, after which the reclaimed land is ready to become productive again, having its local vegetation and wildlife restored as closely as possible to its original conditions [5,11].

1.2. Water Purification

Water is a precious liquid on which mankind life strongly depends. Nowadays, more than 80 countries around the world are affected by water scarcity, which is expected to affect the life of approximately 2.7 billion people by 2025. It has been predicted that conflicts over water might be severer than that over oil in the future. Even though we know that water is a vital, valuable, and scarce substance, its pollution is the consequence of domestic or industrial activities. Some natural phenomena such as land erosion can also result in dissolving or dispersing contaminant materials in water. Water reclamation is one of the solutions to this problem [12,13].

To reclaim contaminated water, the solid particles dispersed in wastewaters need to be removed in a process called *dewatering*. The solid-liquid separation methods used in dewatering may differ based on the size and type of solid particles dispersed in water. Thickening is used when the size of the particles is big enough to make them settle by gravity. Smaller solid particles, however, are not easily separated by gravity [12,14].

Table 1.1 classifies solid particles based on their sizes, and compares the time required for each category to settle 100 mm in water. Colloidal particles, with 10^{-5} mm diameters or less, tend to remain dispersed in aqueous suspension for several years due to their high surface area per unit volume. The removal of colloidal particles from wastewater needs other technologies rather than gravitational separation [12].

Table 1.1. Classification of particles according to their sizes (adapted from [12]).

Particle size (mm)	Classification	Examples	Total surface area (mm ² /mm ³)	<i>t</i> *
10	Coarse dispersion	Coarse sand	0.6	0.1 s
1			6	1 s
10 ⁻²	Fine particulate dispersion	Silt	600	11 min
10 ⁻⁵	Colloidal dispersion	Mineral substances	6 × 10 ⁵	2 years
10 ⁻⁶			6 × 10 ⁶	20 years
<10 ⁻⁶	Solution	Molecules	—	—

**t*: time required for the particles with specific gravity of 2.65 to settle 100 mm.

Not only the size of the particles, but also their surface charges, may enhance their ability to remain dispersed in water. Charged particles generally occur in aqueous suspensions due to several factors such as ionization of functional groups, adsorption of ions, and dipole orientation. Therefore, particles with the same charge remain dispersed in suspension as they repel each other [15].

When the dispersed particles do not settle by gravity, they may be destabilized and/or agglomerated by other means; the larger particles may then be removed by filtration, centrifugation, or allowed to settle down by gravity. Moreover, coagulation and flocculation are processes widely used to destabilize particles dispersed in solutions. Coagulation destabilizes suspended particles, while flocculation aggregates destabilized particles [12,14,16].

1.3. Electric Double Layer Forces

Three repulsive forces – solvation, steric, and electrostatic – disperse solid particles in aqueous medium. Among them, electrostatic forces are the most important because charged particles can be abundantly found in aqueous suspensions [17].

Figure 1.3 shows a negatively charged particle in a suspension. Charged particles adsorb counter-ions to balance their own surface charges. This phenomenon changes the ion distribution around the charged particle compared to the bulk phase, creating a layer of co- and counter-ions around the suspended particle called the *electrical double layer*. The net charge difference between the ion distribution around the particle and the ion distribution in the bulk phase induces an electric potential between the electrical double layer and the bulk phase, as illustrated in Figure 1.3. The electric potential difference between the particle surface and the bulk suspension is called the *Nernst potential* (ψ_0).

Since the surface of the particle in Figure 1.3 is negatively charged, it attracts cations (counter-ions). The adsorbed counter-ions create a layer around the particle surface called the *Stern* or the *Helmholtz layer*, which is the first region of electrical double layer. The second region, called the *diffuse layer*, is located between the Stern layer and the bulk phase, where the concentration of counter-ions is higher than the concentration of co-ions. Moving away from the particle surface, the concentration of counter-ions decreases, and the concentration of co-ions increases in the diffuse layer. The counter-ions and the water molecules in the diffuse layer are mobile, while the counter-ions in the Stern layer are adsorbed on the surface of the particle and do not move. Moreover, there is also a layer of water molecules that is electrostatically bound to the surface of the particle. The water molecules of this layer do not move freely, creating a water-water boundary

with the surrounding mobile water molecules called the *plane of shear*. Because the layer of water molecules bound to the particle surface is very thin, sometimes just a monolayer, it is not shown in Figure 1.3. The electric potential difference between the plane of shear and the bulk solution is called the *zeta potential* (ξ) [16-18].

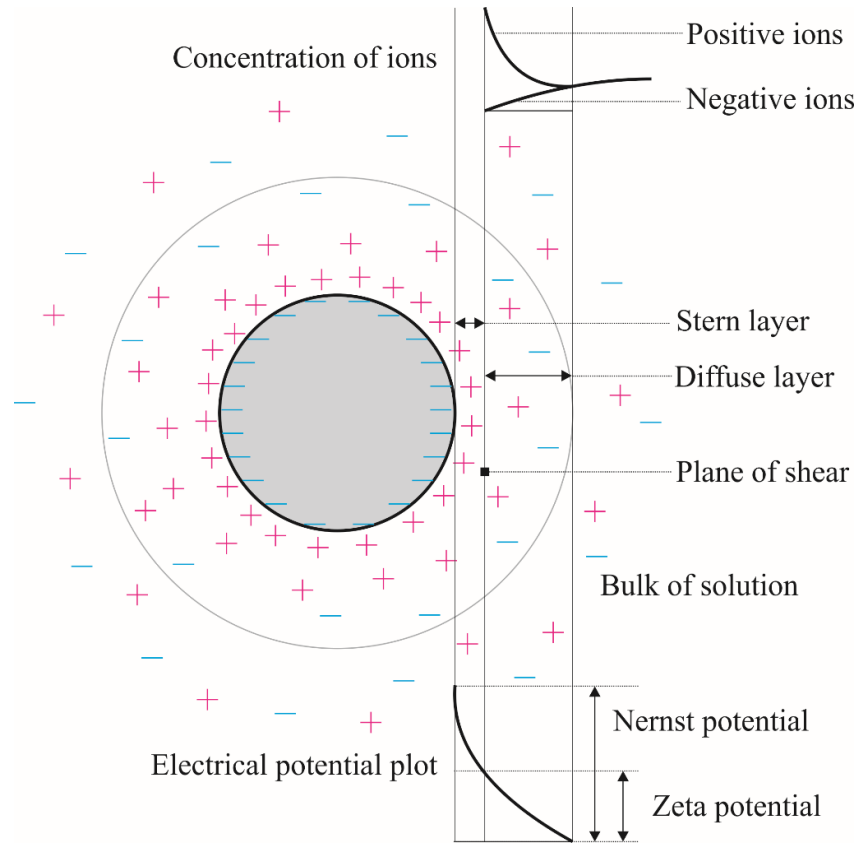


Figure 1.3. Electric double layer of a negatively charged particle in aqueous suspension (redrawn from [16]).

1.4. Colloid Stability and DLVO Theory

The stability of colloidal particles in a suspension depends on the interfacial interactions resulting from both attractive van der Waals and repulsive electrostatic (double layer) forces. The balance between these attractive and repulsive forces was explained by Derjaguin, Landau, Verwey, and Overbeek (DLVO). The DLVO theory estimates the energy of attraction and the energy of repulsion as a function of the distance between particles. Figure 1.4 shows two negatively charged particles approaching each other in a suspension. The attractive (negative) and repulsive (positive) energies are also plotted versus the distance between the particles (approximately <50 nm). The middle curve is the sum of attractive and repulsive energies (DLVO interaction). As the two particles approach each other, the net DLVO interaction increases to a maximum potential energy (point A) called *energy barrier*. At this stage, particles repel each other, stabilizing the suspension. If the thermal kinetic energy of the particles is higher than the energy barrier, however, they may keep getting closer and overcome the energy barrier. As they approach each other, van der Waals attraction forces become predominant, and the particles aggregate [17,18].

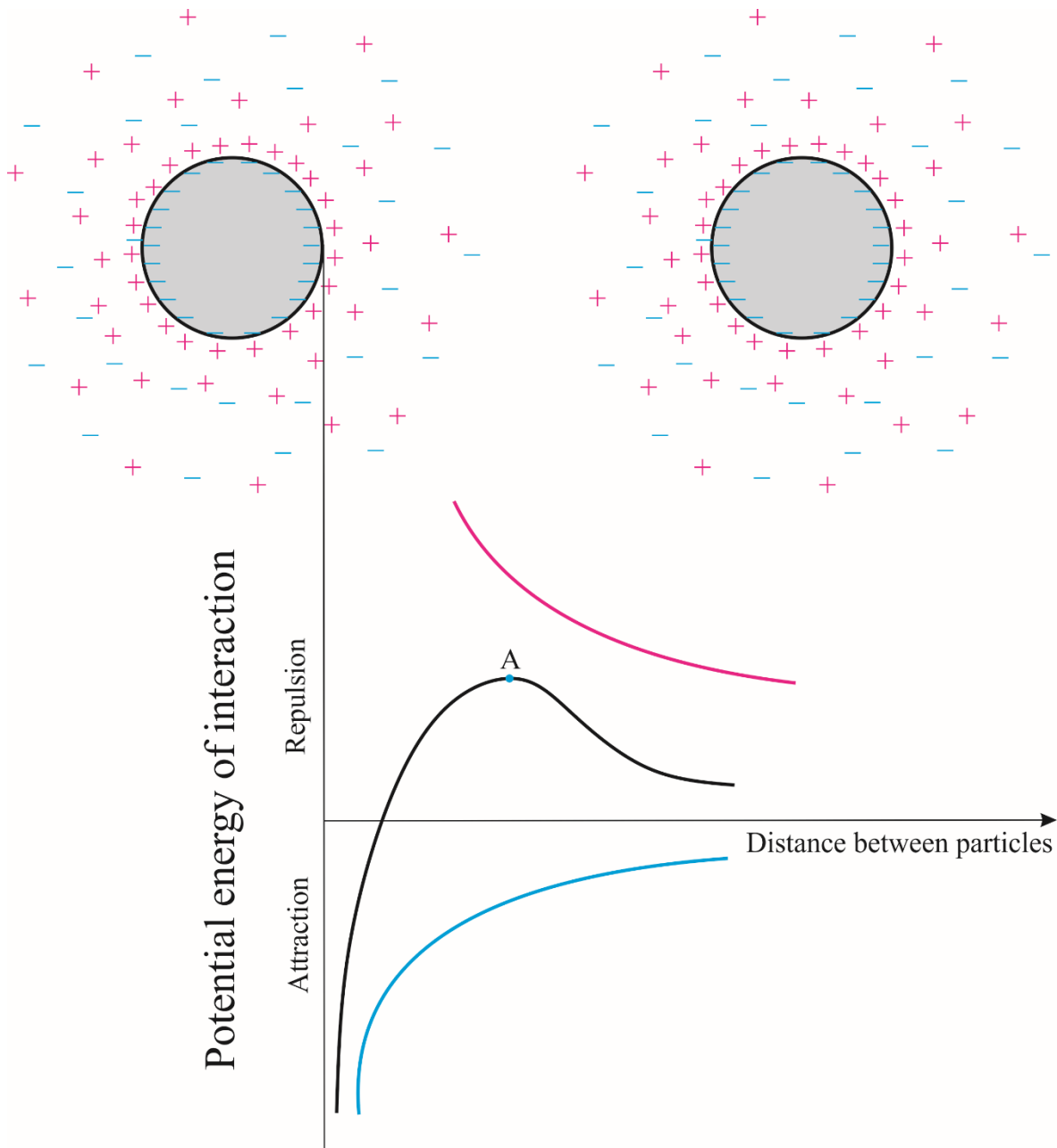


Figure 1.4. Potential energy of interaction versus distance between two negatively charged particles (redrawn from [17,18]).

The following methods may be used to decrease the energy barrier and promote particle aggregation: neutralization of particle surface charges, reduction of the electric double layer thickness, and molecular bridging. Counter ions, such as Al^{3+} , Fe^{3+} , Fe^{2+} , Mg^{2+} , and Ca^{2+} , may be used to reduce surface charge of the particles. The thickness of the double layer may be reduced by adding electrolytes to the suspension, increasing the ionic strength of the suspension and suppressing the formation of the counter-ions cloud around the particles. Finally, the suspended particles may be bridged by adding large molecules, called polymeric flocculants, to the suspension [16,18,19].

1.5. Polymeric Flocculants

In addition to their applications in various fields such as pharmaceuticals, cosmetics, paints, and adhesives, polymers are used widely as coagulants and flocculants in water purification process [20]. Polymers are large molecules made of many small segments called repeating units. Based on the nature of the repeating units, polymers could be non-ionic, cationic, anionic, or amphoteric (containing both cationic and anionic repeating units) [21].

Depending on properties such as molecular weight and charge density, polymers carry out flocculation through different mechanisms, among which *bridging*, *charge neutralization*, and *electrostatic patch* predominate. In all mechanisms, the polymer chains must adsorb onto the surface of the particles. Non-ionic polymers adsorb onto negatively charged particles by hydrogen bonding. As most of the charged particles in suspension carry negative surface charges, polymers with positive charges can adsorb onto their surfaces by electrostatic attraction. Metal cations present on the particle surfaces can also adsorb anionic polymers through salt linkages [15].

Figure 1.5 shows the possible conformations of an adsorbed polymer molecule onto a surface. When a polymer chain is in contact with, or close to, the surface, it makes a *train* configuration. A polymer chain makes a *loop* configuration in between two train segments if it does not have enough space to extend throughout the surface. The polymer chain end, dangling in the bulk phase, is called a *tail* [20,22].

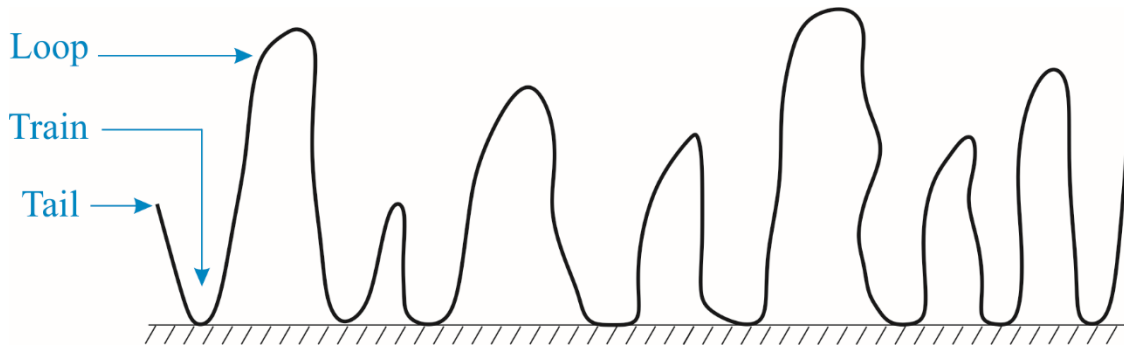


Figure 1.5. Possible configurations of a polymer molecule adsorbed onto a surface.

In the bridging mechanism, when a polymer chain is adsorbed onto a particle, its loops and tails extend into the suspension, where they adsorb onto the surfaces of other particles. This process brings several particles together, forming flocs. By mixing the polymer solution with the particle suspension for a certain period of time, polymer molecules adsorb onto an increasing number of particles, making denser flocs that are more likely to precipitate from the suspension (Figure 1.6) [15,20,23].

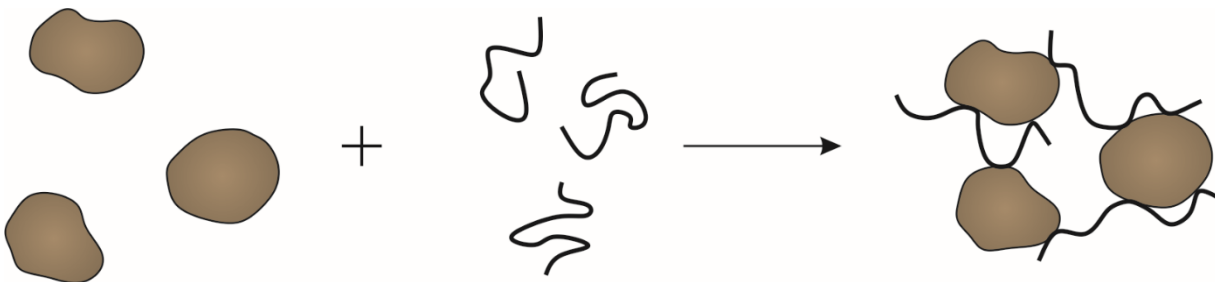


Figure 1.6. Polymer bridging mechanism.

Figure 1.7 illustrates the charge neutralization and electrostatic patch mechanisms. As most particles dispersed in aqueous suspensions are negatively charged, cationic polymers can be used to neutralize their surface charges, reducing the electrostatic repulsion between co-ions. Charge neutralization allows particles to approach each other so that flocs can be formed via attractive van der Waals interactions. Finally, the electrostatic charge patch mechanism occurs when positively charged polymers adsorb on the surface of particles, creating localized positive charges. These particles can electrostatically attract each other because they have both positively- and negatively-charged segments/groups on their surfaces, as shown in Figure 1.7 [23].

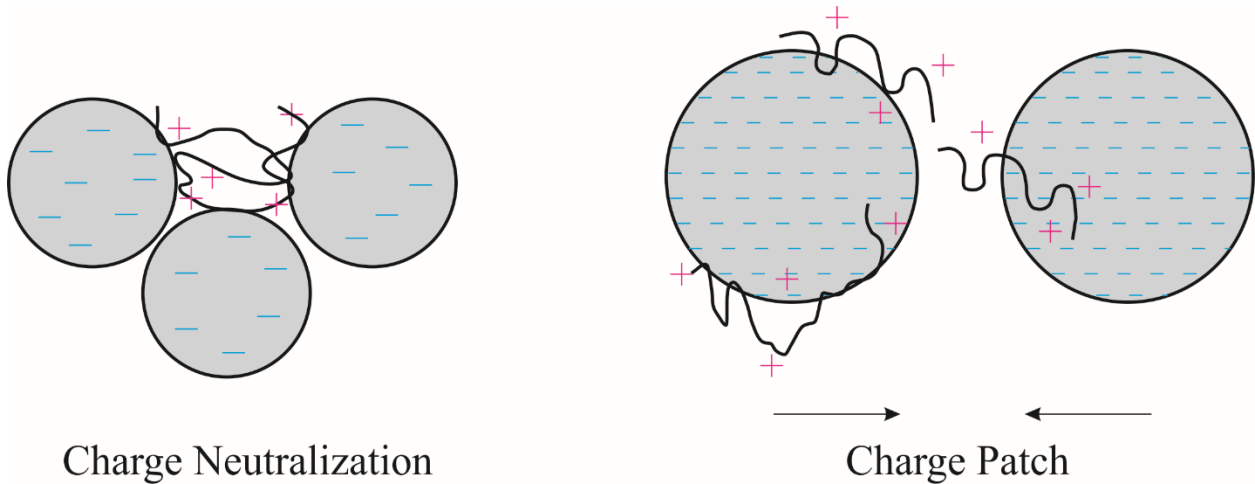


Figure 1.7. Charge neutralization and charge patch mechanisms (redrawn from [23]).

Figure 1.8 illustrates a flocculation experiment. The leftmost cylinder shows dispersed particles in suspension. After mixing the suspension with a polymer flocculant solution, flocs start forming and settling by gravity (central cylinder). The settled flocs are called *sediments*, and the liquid at the top of the sediments is called *supernatant* (rightmost cylinder). The quality of supernatant, the

amount of solid particles remaining in the supernatant, the solids content of the sediments, and the amount of polymer used in the flocculation determine the efficiency of the flocculation process.

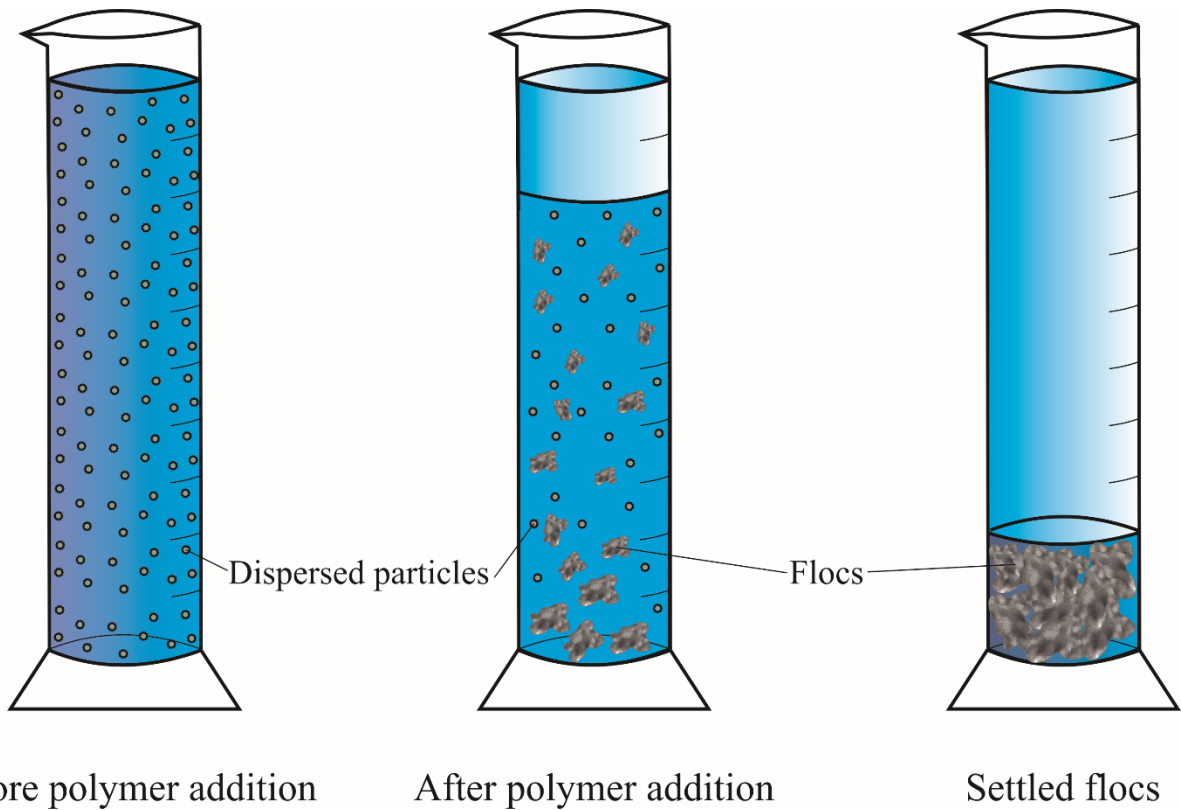


Figure 1.8. Macroscopic schematic for the flocculation process.

1.6. Natural, Synthetic, and Graft Polymers

Polymers may be classified into natural or synthetic polymers. *Natural polymers* are extracted from natural resources, such as plants or animals; *synthetic polymers* are normally derived from petroleum-based chemicals [24]. Either class has been used as flocculants in water purification. Starch, chitosan, cellulose, guar gum, and sodium alginate are some examples of the most important natural flocculants [21,23]. Among synthetic polymers, polyacrylamide (PAM), polyacrylic acid (PAA), poly(methyl acrylate) (PMA), poly(methyl methacrylate) (PMMA), poly(diallyl dimethyl ammonium chloride) (DADMAC), and polyethylene oxide (PEO) are widely used as flocculants [15].

Compared to synthetic polymers, natural polymers are renewable, inexpensive, environmental friendly, and fairly shear stable. However, synthetic polymers are more efficient flocculants and also have longer shelf lives [23]. Molecular weight, molecular weight distribution, polymer structure, and ionicity affect the performance of polymers as flocculants [15]. These properties are easy to adjust in synthetic polymers to improve their flocculation behavior. The flocculation ability of natural flocculants may also be improved by chemical modifications. One of the widely used modification method is to graft synthetic polymers onto the backbone of natural polymers [23], thus combining the attractive properties of both polymer classes in a single molecule.

Graft polymers of synthetic and natural polymers have branched structures. Typically, the backbone is made of the rigid natural polymer, and the grafts consist of flexible synthetic polymer chain. Figure 1.9 compares the structure of a linear and a branched polymer. The side chains dangling from the backbone are more likely to flocculate the suspended particles than the coils of the linear polymer (Singh's approachability model). Moreover, grafting the synthetic polymer onto

the natural polymer backbone increases its molecular weight. Graft polymers are still shear stable, and benefit from the low cost and renewability of natural polymers [23,25].

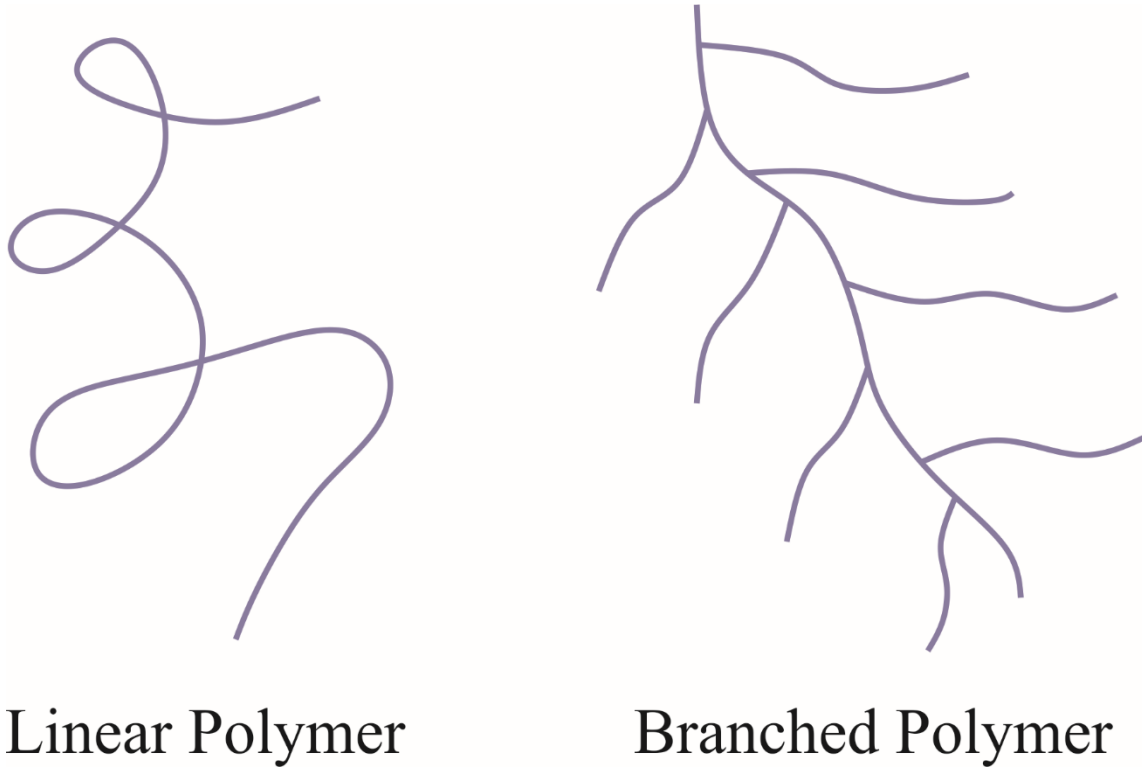


Figure 1.9. Linear polymer and graft (branched) polymer in a suspension (redrawn from [25]).

1.7. Amylopectin Grafted Flocculants

Starch is a natural polymer that has been extensively used as the backbone of graft polymer flocculants because of its low cost and availability. Starches can be extracted from several sources, such as corn (maize), wheat, rice, and potato, which affects their appearance, properties, and compositions. Starch is a polymer from the polysaccharides family (formed by glucose units), which is among the most abundant natural resources worldwide [24]. Starch molecules are formed by two different polymers called *amylose* and *amylopectin* (AP). Amylose is a linear polymer, but amylopectin is highly branched, as shown in Figure 1.10 [26,27]. Both have been used as backbones in graft polymers. Compared to amylose, amylopectin-grafted polymers are likely to perform better as flocculants because of their long branches and higher molecular weights [25].

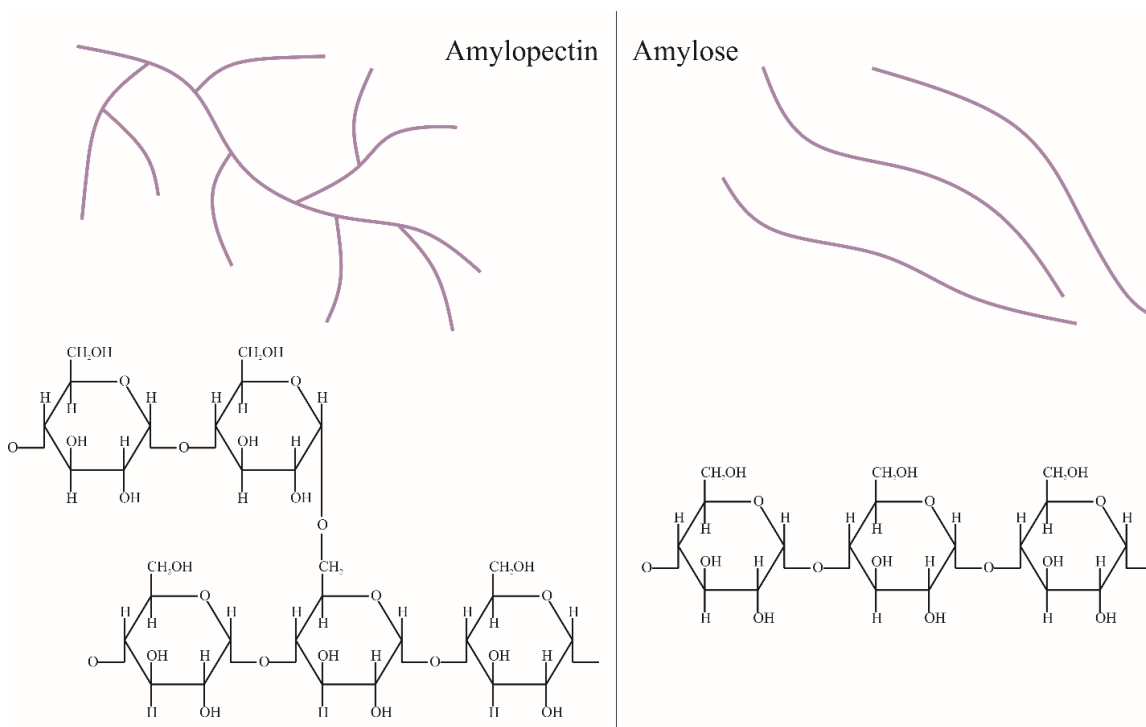


Figure 1.10. Structure of amylopectin and amylose (redrawn from [26,27]).

The common method used to graft synthetic polymers onto natural backbones is called *grafting-from* (Figure 1.11). In this technique, free radicals are produced on the backbone of the natural polymer, from which the grafts grow in the presence of monomers through free radical polymerization or other mechanism [28,29]. Several techniques have been developed to produce free radicals on these backbones. Free radical initiators or microwave irradiation have been widely used to synthesize amylopectin-graft polymers [30]. Ceric ammonium nitrate (CAN) [31], potassium persulfate (KPS) [32], and ammonium persulfate (APS) [33] are free radical initiators used to graft polymer chains onto amylopectin backbone.

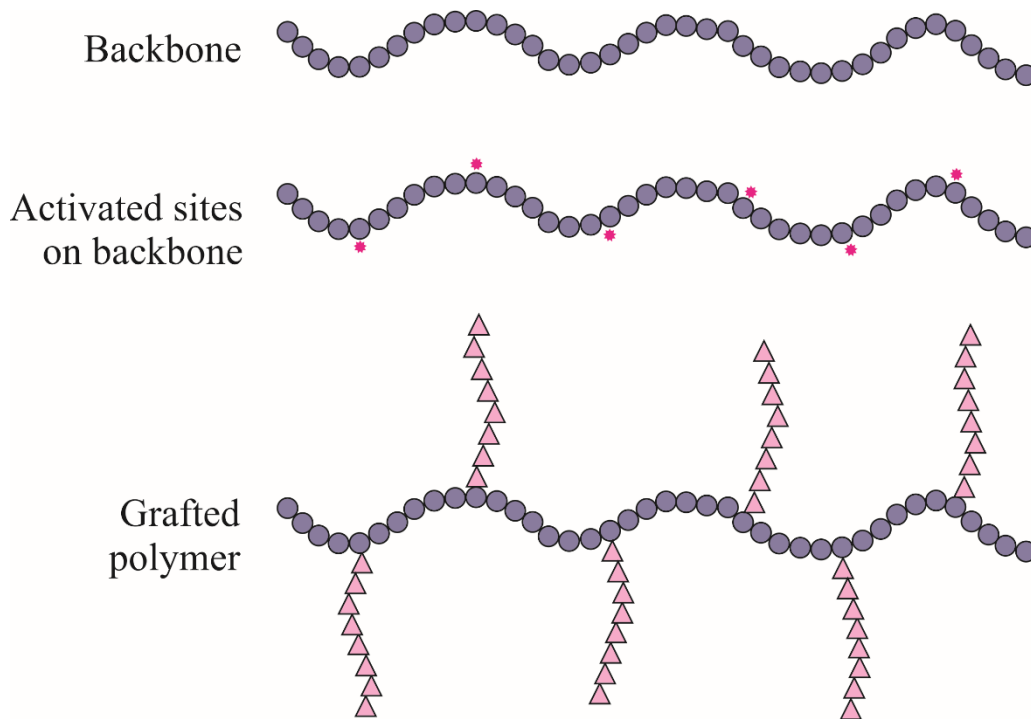


Figure 1.11. Schematic of polymerization through grafting-from method.

Different synthetic polymers have been grafted onto amylopectin, such as polyacrylamide and poly(N,N-dimethylacrylamide) (PDMA). Amylopectin-grafted PDMA (AP-g-PDMA) is a better flocculant than AP-g-PAM for diluted coal, silica, kaolin, and iron ore suspensions, because the PAM grafts form strong intramolecular hydrogen bonds between NH₂ and C=O groups of the adjacent amide groups, which restricts the solubility of the polymer in water, and consequently reduces the approachability of the chains to particles dispersed in the suspension. Moreover, the amide groups in the PDMA chains are more polar due to presence of methyl groups attached to nitrogen atoms, and attract colloidal particles more efficiently due to their partially charged sites [31,34].

Poly(methyl acrylate) is another synthetic polymer that has been grafted onto amylopectin and used to absorb cadmium ions. However, because PMA is insoluble in water, the methyl acrylate groups of the synthesized AP-g-PMA must be hydrolyzed in sodium hydroxide solution before being used as a flocculant. Samsal et al. have synthesized AP-g-poly(methyl acrylate-co-sodium acrylate) by partially hydrolyzing the methyl ester (–COOCH₃) groups and transforming them to the sodium acrylate (–COONa) groups, which makes the graft polymer soluble in alkaline water [35].

Amylopectin grafted poly(acrylic acid) (AP-g-PAA) was also used as flocculant for synthetic iron ore, manganese ore, and kaolin suspensions [32]. AP-g-PAA is not completely soluble in water due to its intramolecular hydrogen bonding between carboxylic acid groups, but it can become more soluble at alkaline pH [35].

It is also possible to use more than one monomer type in graft polymerization. To graft PAA and PAM onto AP, the AP-g-PAM was synthesized and used in second polymerization to graft PAA chains on the backbone. The inclusion of PAA and PAM grafts increased the molecular weight of

the polymer and enhanced flocculation performance of (AP-*g*-PAM)-*g*-PAA for 0.25 wt.% iron ore suspensions. In fact, it increased the repulsive interactions between the dangling chains, its hydrodynamic volume, and consequently the approachability of the grafts by the suspended particles [36].

If more than one monomer type is added to the polymerization reactor simultaneously during the grafting process, the polymer of those monomers would form graft onto the AP backbone. Samsal et al. used acrylamide and N-methyl acrylamide simultaneously to synthesize amylopectin-*g*-poly(acrylamide-co-N-methyl acrylamide). Flocculation tests performed in diluted coal, silica, kaolin, iron ore, and bentonite clay suspensions showed that AP-*g*-poly(AM-co-NMA) performed better than AP-*g*-PAM. The presence of N-methyl amide units in the grafted chains decreased hydrogen bonding between AM units and made the chains more flexible and approachable to fine particles [37].

To synthesize amphoteric AP-*g*-PAM, negative charges were produced by hydrolyzing the CONH₂ groups of PAM chains in NaOH solution. Moreover, 3-chloro-2-hydroxypropyl trimethylammonium chloride (CHPTAC) was used to introduce cationic moieties onto the backbone of the hydrolyzed graft polymer in the presence of sodium hydroxide. Amphoteric AP-*g*-PAM performed better than hydrolyzed and unmodified AP-*g*-PAM for the flocculation of kaolin and iron ore suspensions [30].

In another work, the cationic monomer (3-acrylamidopropyl) trimethylammonium chloride (ATMAC) and acrylamide were simultaneously used in graft polymerization to synthesize cationic graft polymer. Sodium hydroxide was used to hydrolyze some of the acrylamide groups and create negatively-charged segments on the polymer. The final amphoteric polymer had PAM, hydrolyzed

PAM, and PATMAC grafts, and was used to remove dyes and to flocculate kaolin suspensions [33].

Generally, the monomer type and charge of the graft polymers have significant effects on the flocculation performance of AP graft polymers. The length and the frequency of the grafts also affect the flocculation performance of graft polymers [38]. Table 1.2 summarizes the published results of AP graft polymers used as flocculants. As their performances have been evaluated mostly for the flocculation of synthetic waste waters, one would ask whether these flocculants are efficient to dewater actual wastewaters coming from different mining processes, as the water chemistry, presence of organic materials, and types of solids may differ substantially from model systems.

The main objective of this thesis is to synthesize AP graft polymers and use them to dewater Alberta's oil sands tailings for the first time, to find out whether they can conquer the challenges that Alberta's oil sands industry is currently facing.

Table 1.2. Amylopectin grafted polymers used as flocculants.

No.	Polymer	Waste water	Ref.	Year
1	AP-g-PDMA	1 wt. % coal	[31]	2014
	AP-g-PAM	1 wt. % silica		
2	AP-g-PDMA	1 wt. % kaolin clay	[34]	2013
	AP-g-PAM	0.25 wt. % iron ore slime		
3	AP-g-PAA	Iron ore, manganese ore, and kaolin suspensions	[32]	2013
4	AP-g-PHPMA	Cadmium ion solution	[35]	2016
5	(AP-g-PAM)-g-PAA	0.25 wt. % iron ore suspension	[36]	2012
6	CHPTAC-AP-g-PHPAM	3 wt. % kaolin 5 wt. % iron ore	[30]	2013
7	AP-g-Poly(AM-co-sodium AM-co- ATMAC)	Kaolin suspension Dye removal (methylene blue)	[33]	2015
8	AP-g-poly(AM-co-NMA)	1.0 wt.% coal 1.0 wt.% silica 1.0 wt.% kaolin 0.25 wt.% iron ore 1.0 wt.% bentonite clay	[37]	2015
9	AP-g-PAM	Synthetic lead effluent	[25]	2000
10	AP-g-PAM	0.25 % kaolin suspension	[39]	1997
11	AP-g-PAM	Coking coal and non-coking coal suspensions	[40]	1998
12	AP-g-PAM	0.25% w/v kaolin suspension White paper-mill effluent	[38]	1998

1.8. References

1. Government of Alberta C. Environmental management of Alberta's oil sands. 2009.
2. Vedoy DR, Soares JB. Water-soluble polymers for oil sands tailing treatment: A Review. The Canadian Journal of Chemical Engineering 2015;93(5):888-904.
3. Masliyah JH, Xu Z, Czarnecki JA, Dabros M. Chapter 1. Introduction to the Athabasca Oil Sands. In: Handbook on Theory and Practice of Bitumen Recovery from Athabasca Oil Sands. Cochrane, Alta.: Kingsley Knowledge Pub., 2011. p. 1-49.
4. Masliyah JH, Xu Z, Czarnecki JA, Dabros M. Chapter 4. Physical and Chemical Properties of Oil Sands. In: Handbook on Theory and Practice of Bitumen Recovery from Athabasca Oil Sands. Cochrane, Alta.: Kingsley Knowledge Pub., 2011. p. 173-266.
5. BGC Engineering Inc., 2010. Oil Sands Tailings Technology Review. Oil Sands Research and Information Network, University of Alberta, School of Energy and the Environment, Edmonton, Alberta. OSRIN Report No. TR-1. 136 pp. .
6. Environmental Defence Canada (EDC) and Natural Resources Defense Council (NRDC). One trillion litres of toxic waste and growing: Alberta's tailings ponds. 2017.
7. Masliyah JH, Xu Z, Czarnecki JA, Dabros M. Chapter 8. Colloidal Science in Tailings Management. In: Handbook on Theory and Practice of Bitumen Recovery from Athabasca Oil Sands. Cochrane, Alta.: Kingsley Knowledge Pub., 2011. p. 391-452.

8. Botha L, Soares JBP. The Influence of Tailings Composition on Flocculation. *Can J Chem Eng* 2015;93(9):1514-1523.
9. Alberta Energy Regulator (<http://www.aer.ca>).
10. Chalaturnyk RJ, Don Scott J, Özüm B. Management of oil sands tailings. *Petrol Sci Technol* 2002;20(9-10):1025-1046.
11. Beier N, Wilson W, Dunmola A, Segó D. Impact of flocculation-based dewatering on the shear strength of oil sands fine tailings. *Canadian Geotechnical Journal* 2013;50(9):1001-1007.
12. Bratby J. Chapter 1. Introduction. In: *Coagulation and Flocculation in Water and Wastewater Treatment* (2nd Edition). London, UK: IWA Publishing, 2006. p. 1-8.
13. Ahuja S. Chapter 1. Overview: Water Reclamation and Sustainability. In: Ahuja S, editor. *Water Reclamation and Sustainability*. Boston: Elsevier, 2014. p. 1-18.
14. Concha A. F. Chapter 1. Introduction. In: Concha A. F, editor. *Solid-Liquid Separation in the Mining Industry*. Cham: Springer International Publishing, 2014. p. 1-10.
15. Williams PA. Chapter 6. Polymeric Flocculants. In: *Handbook of Industrial Water Soluble Polymers*. Oxford ;Ames, Iowa: Blackwell Pub., 2007. p. 134-173.
16. Bratby J. Chapter 2. Colloids and interfaces. In: *Coagulation and Flocculation in Water and Wastewater Treatment*. London, UK: IWA Publishing, 2006. p. 9-30.
17. Israelachvili JN. Chapter 14. Electrostatic Forces between Surfaces in Liquids. In: *Intermolecular and Surface Forces*. Burlington, MA: Academic Press, 2011. p. 291-340.

18. Concha A. F. Chapter 7. Particle Aggregation by Coagulation and Flocculation. In: Concha A. F, editor. Solid-Liquid Separation in the Mining Industry. Cham: Springer International Publishing, 2014. p. 143-172.
19. Scholz M. Chapter 7. Coagulation and Flocculation. In: Scholz M, editor. Wetlands for Water Pollution Control (Second Edition): Elsevier, 2016. p. 37-46.
20. Williams PA. Chapter 1: Introduction. In: Handbook of Industrial Water Soluble Polymers. Oxford ;Ames, Iowa: Blackwell Pub., 2007. p. 1-9.
21. Bratby J. Chapter 3. Coagulants. In: Coagulation and Flocculation in Water and Wastewater Treatment. London, UK: IWA Publishing, 2006. p. 31-71.
22. Bolto B, Gregory J. Organic polyelectrolytes in water treatment. Water Research 2007;41(11):2301-2324.
23. Lee CS, Robinson J, Chong MF. A review on application of flocculants in wastewater treatment. Process Saf Environ Prot 2014;92(6):489-508.
24. Olatunji O. Chapter 1. Classification of Natural Polymers. In: Natural Polymers : Industry Techniques and Applications. Cham: Springer, 2016. p. 1-17.
25. Singh RP, Karmakar GP, Rath SK, Karmakar NC, Pandey SR, Tripathy T, Panda J, Kanan K, Jain SK, Lan NT. Biodegradable drag reducing agents and flocculants based on polysaccharides: Materials and applications. Polym Eng Sci 2000;40(1):46-60.

26. Rutenberg MW. Starch and Its Modifications. In: Handbook of Water-Soluble Gums and Resins. : New York : McGraw-Hill, c1980, 1980. p. 1-6.
27. Kennedy JF, Knill CJ, Liu L, Panesar PS. Starch and its Derived Products: Biotechnological and Biomedical Applications. In: Renewable Resources for Functional Polymers and Biomaterials: Polysaccharides, Proteins and Polyesters. : The Royal Society of Chemistry, 2011. p. 130-165.
28. Bonilla-Cruz J, Dehonor M, Saldívar-Guerra E, González-Montiel A. Chapter 10. Polymer Modification: Functionalization and Grafting. In: Handbook of Polymer Synthesis, Characterization, and Processing. : John Wiley & Sons, Inc., 2013. p. 205-223.
29. Singh V, Kumar P, Sanghi R. Use of microwave irradiation in the grafting modification of the polysaccharides—A review. Progress in polymer science 2012;37(2):340-364.
30. Singh RP, Pal S, Rana VK, Ghorai S. Amphoteric amylopectin: A novel polymeric flocculant. Carbohydr Polym 2013;91(1):294-299.
31. Kolya H, Tripathy T. Biodegradable flocculants based on polyacrylamide and poly(N,N-dimethylacrylamide) grafted amylopectin. Int J Biol Macromol 2014;70:26-36.
32. Sarkar AK, Mandre N, Panda A, Pal S. Amylopectin grafted with poly (acrylic acid): Development and application of a high performance flocculant. Carbohydr Polym 2013;95(2):753-759.

33. Kumar K, Adhikary P, Karmakar N, Gupta S, Singh RP, Krishnamoorthi S. Synthesis, characterization and application of novel cationic and amphoteric flocculants based on amylopectin. *Carbohydr Polym* 2015;127:275-281.
34. Kolya H, Tripathy T. Grafted polysaccharides based on acrylamide and N, N-dimethylacrylamide: Preparation and investigation of their flocculation performances. *J Appl Polym Sci* 2013;127(4):2786-2795.
35. Sasmal D, Kolya H, Tripathy T. Amylopectin-g-poly(methylacrylate-co-sodium acrylate): An efficient Cd(II) binder. *Int J Biol Macromol* 2016;91:934-945.
36. Pal S, Pal A. Synthesis and characterizing a novel polymeric flocculant based on amylopectin-graft-polyacrylamide-graft-polyacrylic acid [(AP-g-PAM)-g-PAA]. *Polymer bulletin* 2012;69(5):545-560.
37. Sasmal D, Singh R, Tripathy T. Synthesis and flocculation characteristics of a novel biodegradable flocculating agent amylopectin-g-poly (acrylamide-co-N-methylacrylamide). *Colloids Surf Physicochem Eng Aspects* 2015;482:575-584.
38. Rath S, Singh R. Grafted amylopectin: applications in flocculation. *Colloids Surf Physicochem Eng Aspects* 1998;139(2):129-135.
39. Rath SK, Singh RP. Flocculation characteristics of grafted and ungrafted starch, amylose, and amylopectin. *J Appl Polym Sci* 1997;66(9):1721-1729.

40. Karmakar NC, Rath SK, Sastry BS, Singh RP. Investigation on flocculation characteristics of polysaccharide-based graft copolymers in coal fines suspension. *J Appl Polym Sci* 1998;70(13):2619.

Chapter 2: Materials and Methods

2.1. General

In this chapter, synthesis of AP-g-PAM, polymer and MFT characterization methods, and flocculation tests are described.

2.2. Experimental

2.2.1. Materials

Amylopectin (AP) from maize, ceric (IV) ammonium nitrate (CAN) ($\geq 98.5\%$), acrylamide (AM) ($\geq 98\%$), acetic acid ($\geq 99.7\%$), and toluene (99.9%) were purchased from Sigma-Aldrich. Acetone and formamide were purchased from Thermo Fisher Scientific. Two commercial polyacrylamides (PAM), used as reference flocculants, were obtained from Sigma-Aldrich (CP₁, MW = 5-6 MDa) and Kemira (CP₂, MW >10 MDa). The mature fine tailings (MFT) used for flocculation studies were received from Coanda Research and Development Corporation.

2.2.2. Synthesis and Preparation of AP-g-PAM Flocculants

The first step in the AP-g-PAM synthesis was to dissolve the desired amount of AP (Table 2.1) in deionized (DI) water. Because AP does not dissolve in cold water, a mixture of AP and water was heated up to boiling temperature and kept at that temperature for approximately 20 minutes under

reflux until the mixture became clear [1]. The AP solution was cooled down, transferred to a conical flask, and capped with a rubber septum (Figure 2.1). The solution was then purged with nitrogen using two separate needles for nitrogen inlet and outlet. This process continued for 1 h to assure the solution was completely deoxygenated. During this step, the solution temperature was kept constant at 50 °C using an oil bath and a hot plate, and the solution was continuously mixed.

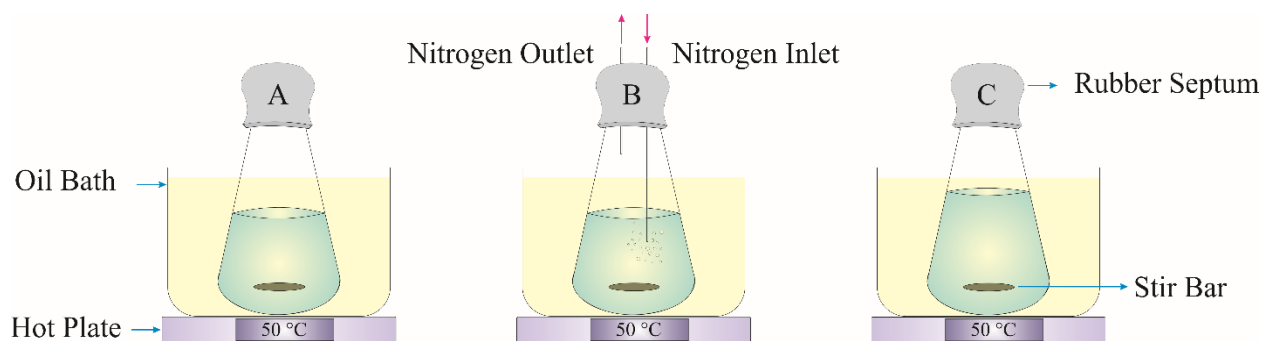
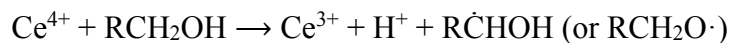


Figure 2.1. Scheme of polymerization set-up.

Afterwards, a freshly prepared solution of CAN, with the chemical formula of $(\text{NH}_4)_2\text{Ce}(\text{NO}_3)_6$, was injected into the polymerization flask. The mass of CAN injected was calculated based on the desired concentrations for each polymerization shown in Table 2.1. Mixing continued for another 15 min to let the initiator attack the AP backbone and form grafting sites on it. At this stage, it is possible for cerium (IV) ion (Ce^{4+}) and the amylopectin alcohol groups, as an organic-inorganic redox pair, to react and produce free radicals by participating in the following dissociation reaction [2],



Then, a deoxygenated solution of acrylamide (Table 2.1) was transferred into the polymerization flask, the flask was carefully sealed, and nitrogen flow was stopped. The total volume of the polymerization solution was equal to 100 ml for all polymerizations. The graft polymerization was continued for 24 h at 50 °C to reach high monomer conversion. At the end of the polymerization, AP-g-PAM was precipitated and washed in excess acetone to remove any unreacted acrylamide. Finally, the precipitated graft polymer was dried in a vacuum oven at 50 °C.

Different grades of AP-g-PAM were synthesized by changing the AM, AP, and CAN concentrations. Table 2.1 shows the details of each polymerization. Each polymer is shown with a code in the second column of Table 2.1. The letter “G” stands for graft polymer. The first number following the letter G is the concentration of AP in the reactor, calculated based on *anhydroglucose unit* (AGU, MW = 162.15 g/mol) and multiplied by 100. AP was varied between 0.7, 1, and 1.4 g; the maximum mass of AP was chosen based on the literature to make sure it did not exceed the solubility limit of AP [3].

The second number in polymer codes shows the ratio of monomer concentration to initiator concentration divided by 1,000. The ratio of backbone to initiator concentrations determine the frequency of PAM grafts on AP, while the ratio of monomer to initiator concentration affects the length of the grafts. Higher monomer to initiator ratios may result in longer grafts and higher molecular weights for AP-g-PAM. To study the effects of these parameters on the flocculation ability of AP-g-PAM, the AM concentration was varied from 0.1 to 1 M, and two different concentrations were used for CAN, 2×10^{-3} and 2×10^{-4} M. Table 2.1 also shows the weight percentage of AP used in the polymerizations. The highest fraction of AP in polymerizations was 49.61 wt.% for G-4-0.5.

Table 2.1. Concentrations of different reagents for the synthesis of AP-g-PAM.

No.	AP-g-PAM	AP (mol AGU/L)	CAN (mol/L)	AM (mol/L)	AP (wt.%)	[M]/[I]*	[M]/[I] ^{0.5}
1	G-4-0.25	0.04	2×10 ⁻³	0.5	16.45	250	11.18
2	G-4-2.5	0.04	2×10 ⁻⁴	0.5	16.45	2500	35.36
3	G-4-0.5	0.04	2×10 ⁻⁴	0.1	49.61	500	7.07
4	G-4-1.5	0.04	2×10 ⁻⁴	0.3	24.71	1500	21.21
5	G-6-3.5	0.06	2×10 ⁻⁴	0.7	16.73	3500	49.50
6	G-6-2.5	0.06	2×10 ⁻⁴	0.5	21.95	2500	35.36
7	G-8-3.5	0.08	2×10 ⁻⁴	0.7	21.95	3500	49.5
8	G-8-2.5	0.08	2×10 ⁻⁴	0.5	28.25	2500	35.36
9	G-8-5	0.08	2×10 ⁻⁴	1	16.45	5000	70.71

*Monomer to initiator ratio

Because PAM homopolymer could also be produced during graft polymerization, the homopolymers were extracted using acetic acid and formamide solvent (1:1 v/v). The unpurified graft polymers were stirred in acetic acid and formamide overnight to let the ungrafted PAM chains dissolve in the solvent. The solution of PAM in acetic acid and formamide was decanted, and the same procedure was repeated two more times for the graft polymer to make sure most of the synthesized PAM chains were separated from the purified graft polymers. Then, the purified AP-g-PAM was separated, dried in vacuum oven, and used in characterization tests [1]. The extracted PAM was precipitated in acetone, collected, and weighed. However, normally the mass of extracted PAM was too small. Therefore, the purified AP-g-PAMs were used only for characterization tests, not for flocculation tests, as the extraction of a very small fraction of PAM was considered not to change its flocculation performance.

To compare the performance of AP-g-PAM with PAM homopolymers, three grades of PAM made with AM/CAN ratios of 2500, 3500, and 5000 were synthesized. Table 2.2 shows the polymerization conditions used to make these homopolymers [4]. Each polymer code starts with

a letter “H” that stands for homo-polymer, followed by a number that shows the monomer to initiator ratio divided by 1,000. Although AP was of course not used to make in PAM homopolymers, all the polymerization conditions were kept similar to those used to synthesize AP-*g*-PAM.

Table 2.2. Concentrations of different reagents for the synthesis of PAM.

No.	PAM	CAN (mol/L)	AM (mol/L)	[M]/[I]*	[M]/[I] ^{0.5}
1	H-2.5	2×10 ⁻⁴	0.5	2500	35.36
2	H-3.5	2×10 ⁻⁴	0.7	3500	49.50
3	H-5	2×10 ⁻⁴	1	5000	70.71

*Monomer to initiator ratio

2.2.3. Polymer Characterization Tests

Fourier Transform Infrared Spectroscopy (FTIR)

Fourier transform infrared spectroscopy (FTIR) was used to confirm the presence of characteristic functional groups in the polymer samples through attenuated total reflection (ATR) method using Agilent Cary 600 FTIR spectrometer. All the samples were scanned with 16 runs and the data was collected from 400 cm^{-1} to 4000 cm^{-1} wavenumbers.

Nuclear Magnetic Resonance Spectroscopy (NMR)

The Agilent/Varian Inova three-channel 400 MHz spectrometer was used for proton (^1H) and carbon (^{13}C) nuclear magnetic resonance spectroscopy (NMR). Samples were first dissolved in deuterium oxide (D_2O), and tests were performed at 27 °C.

Thermogravimetric Analysis (TGA)

A Thermo Cahn analyzer (Thermax 300) was used for thermogravimetric analysis (TGA) of the polymers. The data was collected while the temperature was increasing from 55 to 720 °C, with a heating rate of 10 °C/min under argon atmosphere.

Scanning Electron Microscopy (SEM)

The surface morphology of the polymers was studied by scanning electron microscopy (SEM) after the polymer powder samples had been gold coated in a Denton gold sputter unit. SEM images were taken using either Tescan Vega 3 instrument or Zeiss Sigma (Gemie) field emission-scanning electron microscope (FE-SEM).

2.2.4. MFT Characterization Tests

As each MFT sample could have different characterizations, the MFT characterization tests have been done so that the flocculation results can be compared with future studies.

Moisture Analysis

To measure the solid content of MFT, a MB45 moisture analyzer was used after mixing the sample properly. Three different runs were performed, and the average of results was used to determine the solids content of MFT.

Dean-Stark Extraction

Figure 2.2 shows the scheme of Dean-Stark apparatus which was used to separate water, solid, and bitumen contents of MFT. An undiluted MFT sample was weighed and poured in a thimble. A long-neck round-bottom flask was half filled with toluene, as a solvent to extract bitumen, and the

thimble was hanged inside the flask. The flask was then heated up to boil the toluene. Evaporated toluene passed through the thimble along its way to a condenser, heating up the MFT sample.

As the systems heated up, MFT water evaporated and was collected from the Dean-stark trap after being condensed. The condensed toluene dissolved bitumen on its way back to the flask, and the MFT solids remained in the thimble. This process was allowed to proceed for at least 10 h, and was stopped when the condensed toluene seemed clear after passing through the thimble, confirming that there was no appreciable amount of bitumen in the sample. When the set-up cooled down, the thimble was removed from the flask, and dried completely in a vacuum oven before being weighed. The weight of bitumen extracted by toluene was measured after the toluene was evaporated completely in a vacuum oven. At the end of the experiment, the water, solids, and bitumen contents of MFT could be calculated.

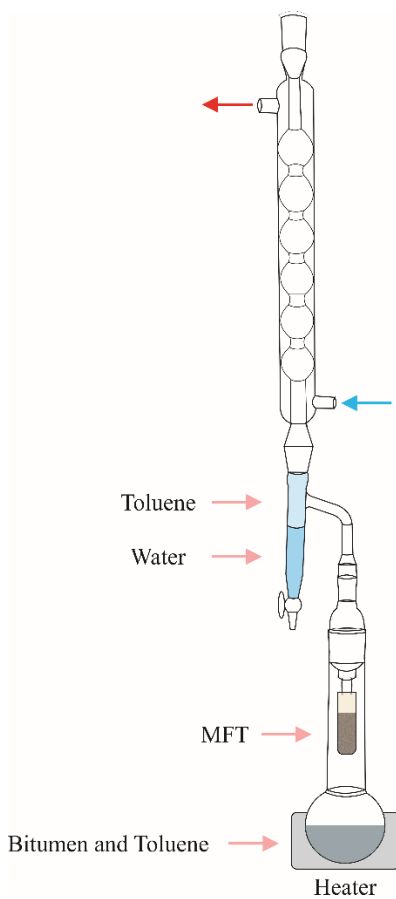


Figure 2.2. Dean-stark apparatus.

Particle Size Distribution (PSD)

Particle size distributions of MFT samples were measured with a Malvern Mastersizer 3000 particle sizer.

Atomic Absorption Spectrophotometry (AAS)

Atomic absorption spectrophotometry (AAS) was used to measure the composition of ions present in the MFT sample. An undiluted MFT sample was centrifuged, the supernatant was collected and

used for the AAS test. A VARIAN 220 FS atomic absorption spectrophotometer and hollow cathode lamp (HCL) light source were used in this technique. Nitrous oxide-acetylene flame for calcium ion, and air-acetylene flame for sodium, potassium, and magnesium ions were utilized.

2.2.5. Flocculation Tests

Jar Test

MFT samples had initially 38 wt.% solids, and were diluted with DI water to 5 wt.% solids for the flocculation tests. The MFT suspension was prepared in a 250 ml beaker and mixed with the polymer solution with a three-blade impeller at 400 rpm for 1 minute. The polymer solution was made in DI water with concentration of 0.002 g/ml. Because the preliminary results showed that large flocs form very fast at AP-g-PAM dosages more than 6,000 ppm, the total mixing time was deliberately kept short to prevent breakage of flocs after their formation. The total volume of the MFT and AP-g-PAM suspension was kept constant at 100 ml. To do so, less water was needed to dilute MFTs at high AP-g-PAM dosages. Polymer dosages were calculated based on the solids content of samples; ppm shows the ratio of dried polymer weight, in mg, to MFT solids weight, in kg.

After the mixing was performed, a volume of approximately 5 ml of the suspension was used to measure capillary suction time (CST). CST showed how fast water was released from the suspension, and was measured by a Triton Type 319 Multi-purpose CST. Samples were poured in an open cylinder of approximately 2.5 cm tall and 2 cm diameter, which was fixed on a filter paper.

The water contained in the sample flowed uniformly by capillarity on the filter paper, and the equipment measured the required time for the water to spread between two sensors that were placed on top of the filter paper. The shorter the time required for water to spread on the filter paper, the better the dewaterability of the samples would be. The measurement was repeated three times and the average of these measurements were reported, and their standard error of the mean was calculated and used as error bars in the plots.

The remaining of the suspension was poured into graduated cylinder and left to rest for 24 h. At this stage, the settling rate of flocs should have been measured; however, because of the fast formation of large flocs at high polymer dosages, no settling could be observed. After 24 h, the supernatant was collected, and the turbidities were measured by a Hach 2100AN turbidimeter. Turbidities were reported by Nephelometric Turbidity Units (NTU). A calibration curve has been prepared and presented in Appendix A to show how turbidities of our MFT samples change with solid contents. Solids content (wt.%) and CST of sediments were also measured to show how much water was in the sediment and how fast it could be released. Sediments were normally separated into four parts: two parts were used to perform two CST tests, and the other two parts were used to measure solids content. The error bars in CST plots of sediments were calculated based on these measurements, which represented operational and equipment errors. To measure solid contents, first, two small plates were made from aluminum foils and weighed. The sediments were placed on the plates and weighed again, before becoming completely dried in a vacuum oven at 50 °C. The samples were weighed again after 24 h, and the weight percentages of solids in the sediments were calculated. The errors reported in the solids contents plots are operational errors.

Sieve Test

Sieve tests were performed to study the natural ability of flocs to release water. MFT samples were diluted to 10 wt.% solid, and the rest of flocculation step was the same as jar tests. However, after mixing step, a 1 mm mesh Fisherbrand U.S.A. Standard Test Sieve was used to separate the supernatant from flocculated MFT. The flocs were left on top of the sieve, and their solids contents were measured right after the flocculation test, after 30 min, and after 1 h. All the flocculation and sieve tests results are presented in Appendix B.

2.3. References

1. Wang J, Yuan S, Wang Y, Yu H. Synthesis, characterization and application of a novel starch-based flocculant with high flocculation and dewatering properties. *Water Res* 2013;47(8):2643-2648.
2. Mino G, Kaizerman S. A new method for the preparation of graft copolymers. Polymerization initiated by ceric ion redox systems. *Journal of Polymer Science Part A: Polymer Chemistry* 1958;31(122):242-243.
3. Kolya H, Tripathy T. Biodegradable flocculants based on polyacrylamide and poly(N,N-dimethylacrylamide) grafted amylopectin. *Int J Biol Macromol* 2014;70:26-36.
4. Erbil C, Gökçeören AT, Polat YO. N-isopropylacrylamide–acrylamide copolymers initiated by ceric ammonium nitrate in water. *Polym Int* 2007;56(4):547-556.

Chapter 3: Results and Discussion

3.1. General

This chapter discusses the characterization of AP-*g*-PAM and MFT as well as flocculation performance of AP-*g*-PAM flocculants.

3.2. AP-*g*-PAM Characterization

3.2.1. Fourier Transform Infrared Spectroscopy (FTIR)

FTIR spectroscopy was performed to confirm the presence of characteristic functional groups in AP, PAM, and AP-*g*-PAM polymers. Table 3.1 lists all the samples used for FTIR.

Table 3.1. FTIR samples.

Sample	Explanation
AP	Commercial amylopectin
PAM	Commercial polyacrylamide (CP ₁)
AP-PAM	Amylopectin (50 wt.%) and polyacrylamide (50 wt.%) blend
AP- <i>g</i> -PAM	Unpurified amylopectin grafted polyacrylamide (unpurified G-4-1.5)
P(AP- <i>g</i> -PAM)	Purified amylopectin grafted polyacrylamide (purified G-4-1.5)

The mass ratio AP/PAM was 1 for the overall the AP-PAM sample. However, due to the inhomogeneity of the AP-PAM mixture (the size of the AP and PAM granules were different in the mixture), different proportion of AP to PAM may has been in contact with IR beam during ATR analysis. FTIR spectra of a purified AP-*g*-PAM, P(AP-*g*-PAM), and an unpurified AP-*g*-PAM were also compared by FTIR. The structures for AP and PAM and the FTIR spectra of all these samples are compared in Figure 3.1. The characteristic wavenumbers and their corresponding functional groups for AP and PAM are listed in Tables 3.2 and 3.3, respectively.

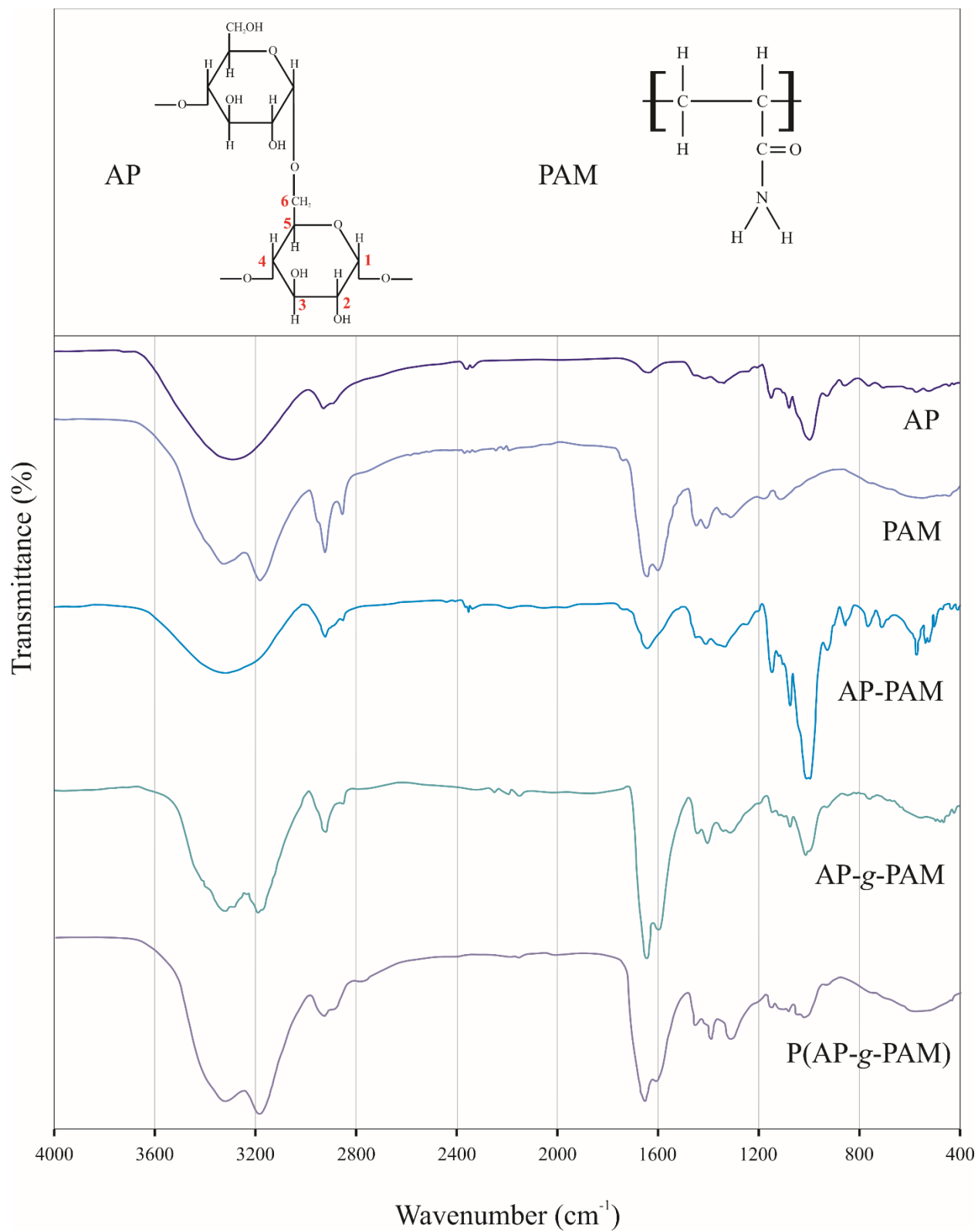


Figure 3.1. FTIR spectra of AP, PAM, AP-PAM, AP-g-PAM, and P(AP-g-PAM).

The first spectrum at the top of Figure 3.1 is for AP. The broad peak at 3300 cm^{-1} may be attributed to the O-H groups in the AP backbone, while the peaks at 1000 and 1100 cm^{-1} may be associated with C-O bonds in C-O-C linkages and C-O-H groups. The C-O-H bending peak was also discernible at 1300 cm^{-1} . Peaks for carbon-hydrogen bonds appear around 2900 cm^{-1} for methanetriyl (C-H) and methylene (C-H₂) groups. The bending peak for methylene groups was observed at 1400 cm^{-1} [1,2].

Table 3.2. Amylopectin characteristic functional groups and their corresponding FTIR wavenumbers.

Functional group	Wavenumber (cm ⁻¹)
O-H	3650-3200
C-O	1300-1000 (stretch)
C-O-H	1440-1220 (bending)
C-H	2900-2800
Methylene (C-H ₂)	~1465 (bending)

The FTIR spectrum for PAM shows a double peak at about 3200 - 3300 cm^{-1} that might be due to presence of NH₂ in the amide groups. The N-H bending peak is observed at 1600 cm^{-1} . Another strong peak, approximately at 1650 cm^{-1} , may be attributed to C=O bonds, but could also confirm the presence of amide group. Moreover, the peaks corresponding to the C-H groups were also discernible at 1400 and 2900 cm^{-1} [1,2].

Table 3.3. Polyacrylamide characteristic functional groups and their corresponding FTIR wavenumbers.

Functional group	Wavenumber (cm ⁻¹)
Primary amide (-NH ₂)	3350 and 3180 (stretch)
Amide (N-H)	1640-1550 (bending)
Amide (C=O)	1680-1630 (stretch)
Methylene (C-H ₂)	~1465 (bending)
C-H	2900-2800

Among all the peaks observed for AP and PAM, the amide peaks are exclusive characteristic peaks for PAM, as there is no amide group in AP. Amongst the peaks associated with amide groups, the strong carbonyl group peak (C=O) and N-H bending peak are more important because AP does not show strong peaks between 1700 to 1500 cm⁻¹. Although there is a weak peak at 1600 cm⁻¹ in the AP spectrum, the shape of the peak is totally different from the peaks observed for amide group at that region. Regarding the AP spectrum, the C-O peak at 1000 cm⁻¹ is important as there is no discernible peak at 1000 cm⁻¹ for PAM. Other peaks for AP and PAM could overlap because they appear in the same regions.

The FTIR analysis may not prove that chemical grafting between AP and PAM took place, but the presence of characteristic peaks for AP and PAM in the AP-*g*-PAM spectrum proves that both AP backbones and PAM chains are present in the AP-*g*-PAM sample. The peaks corresponding to C-O, C=O, and N-H bonds were all present in the AP-*g*-PAM spectrum, which confirmed the presence of AP, C-O, and PAM, C=O and N-H.

No discernible differences between the FTIR spectra for AP-*g*-PAM and AP-PAM was observed in Figure 3.1. This might be because of the low grafting frequency on the AP backbone, making

their peaks very weak, or overlapping of the characteristic grafting peaks with other peaks, which seems to be a more likely explanation.

The spectrum of AP-g-PAM was also compared to that of P(AP-g-PAM) in Figure 3.1 to find out whether material extracted during the purification step affected the FTIR spectrum, and consequently the chemical nature of the product, but no significant difference was observed between AP-g-PAM and P(AP-g-PAM).

3.2.2. Nuclear Magnetic Resonance (NMR)

Figure 3.2 illustrates the chemical structures of AP and PAM. AP has six different carbons in the structure of each glucose unit, and the hydrogens attached to them might show different peaks because of their different environments. Each carbon is identified with a specific number, as shown in Figure 3.2. In structure of PAM, there are three types of hydrogens attached to one nitrogen atom, NH_2 , and two carbon atoms, CH and CH_2 .

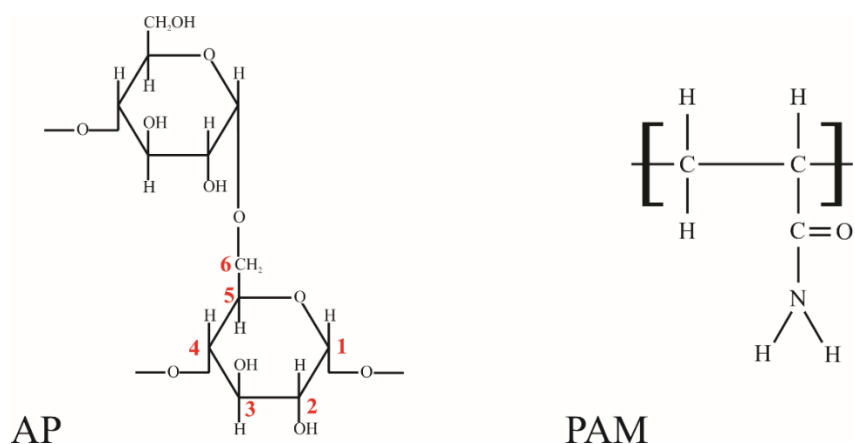


Figure 3.2. AP and PAM structures.

Figure 3.3 shows the ^1H NMR spectrum of AP, PAM, a mixture of AP and PAM (AP-PAM with 25 wt.% AP), and AP-g-PAM. Table 3.4 shows the specifications of each sample used for NMR analysis. The weight percent of AP in the AP-PAM sample was chosen to be close to the weight percentage of AP used in the AP-g-PAM polymerization, 21.95 wt.%.

Table 3.4. NMR samples.

Sample	Explanation
AP	Commercial amylopectin
PAM	Commercial polyacrylamide (CP ₁)
AP-PAM	Amylopectin (25 wt.%) and polyacrylamide (75 wt.%) blend
AP-g-PAM	Unpurified amylopectin grafted polyacrylamide (unpurified G-6-2.5)

The peak at about 4.7 ppm is attributed to hydrogens of deuterium oxide, which was used as solvent. The characteristic chemical shifts of AP are shown in Table 3.5. Hydrogens attached to carbon 6 show their peaks at 3.5 ppm. The chemical shifts related to hydrogens attached to carbons 1 and 4 appeared at 3.7 ppm, and a peak at 3.9 may correspond to hydrogens attached to carbons 2 and 3, in CHOH group, and carbon 5. Chemical shift of hydrogens in hydroxyl group also appeared at 5.3 ppm.

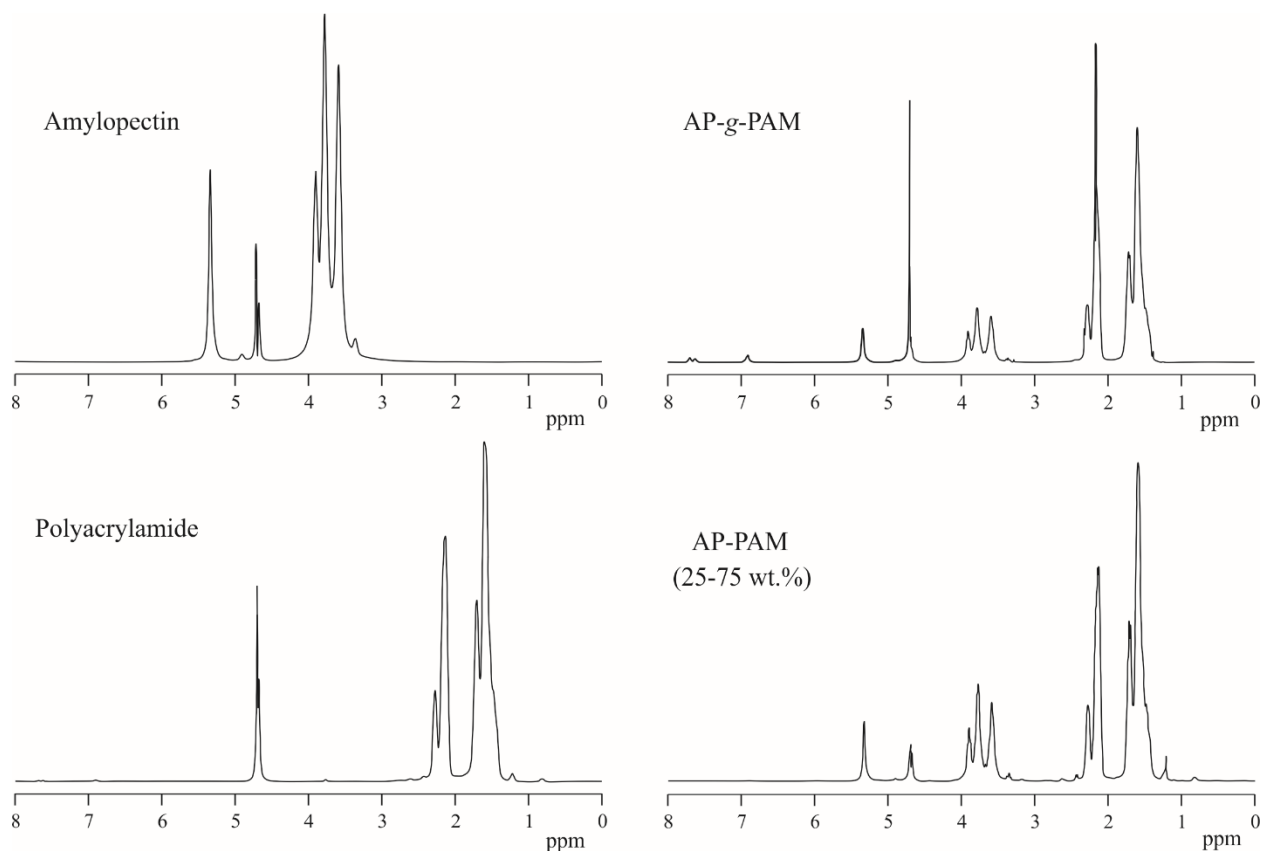


Figure 3.3. Proton NMR chemical shifts for AP, PAM, AP-g-PAM, and AP-PAM.

PAM chemical shifts between 1.2 and 1.8 ppm may be related to hydrogens of methylene group (CH_2), and the peaks at 2-2.4 ppm may be attributed to CH groups (Table 3.6). NH protons of amide groups show singlet broad peaks at about 8 ppm, and each hydrogen attached to nitrogen give a separate peak [3]. So, the weak peaks at 6.9 and 7.6 might be attributed to two NH protons of acrylamide [4-11].

Table 3.5. Amylopectin functional groups and their corresponding ¹H NMR chemical shifts.

Functional Group	Chemical Shift (ppm)
Hydrogens attached to C ₆ (CH ₂ O & CH ₂ OH)	3.5
Hydrogens attached to C ₁ and C ₄ (CHO)	3.7
Hydrogens attached to C ₂ , C ₃ , and C ₅ (CHOH)	3.9
R-OH	5.3

Table 3.6. Polyacrylamide functional groups and their corresponding ¹H NMR chemical shifts.

Functional Group	Chemical Shift (ppm)
CH ₂	1.2-1.8
CH	2-2.4
NH ₂	6.9 & 7.6

The AP-*g*-PAM sample showed the chemical shifts of AP and PAM, confirming that both AP and PAM were present in the sample. The results from samples AP-*g*-PAM and AP-PAM were compared to find a characteristic peak for AP-*g*-PAM which could differentiate chemically grafted polymers from the blend. The goal was to compare the results with FTIR, as the NMR tests are more accurate and reliable. However, no special peak could be assigned to the graft points of AP-*g*-PAM.

Further investigations were carried out to check whether PAM chains were grafted onto AP backbones by ¹³C NMR. Figure 3.4 shows the ¹³C NMR chemical shifts of AP, PAM, AP-PAM (25 wt.% AP), and AP-*g*-PAM. These samples are the same as ones used for ¹H NMR. Tables 3.7 and 3.8 also list the functional groups and their corresponding ¹³C NMR chemical shifts for AP and PAM, respectively

Chemical shifts of AP carbons appeared between 60 and 100 ppm and can be distinguished easily from PAM carbon peaks because there are no discernible peaks at this region for PAM. The peak

around 182 ppm may be attributed to the chemical shift of carbon in the carbonyl group (C=O) of PAM, and the carbons in CH and CH₂ groups showed the chemical shifts at about 44 and 37, respectively. Both AP and PAM carbon chemical shifts are observed in AP-g-PAM results. Compared to AP-PAM, AP-g-PAM did not show any new peaks to be assigned to graft points.

Table 3.7. Amylopectin functional groups and their corresponding ¹³C NMR chemical shifts.

Functional Group	Chemical Shift (ppm)
C ₁ (anomeric carbon)	99.6
C ₄	76.8
C ₃	72-73
C ₂	71.5
C ₆ & C ₅	71.2
C ₄ (nonreducing end)	69.3
C ₆ (nonreducing end)	60.4

Table 3.8. Polyacrylamide functional groups and their corresponding ¹³C NMR chemical shifts.

Functional Group	Chemical Shift (ppm)
C=O	182
CH ₂	36-38
CH	44

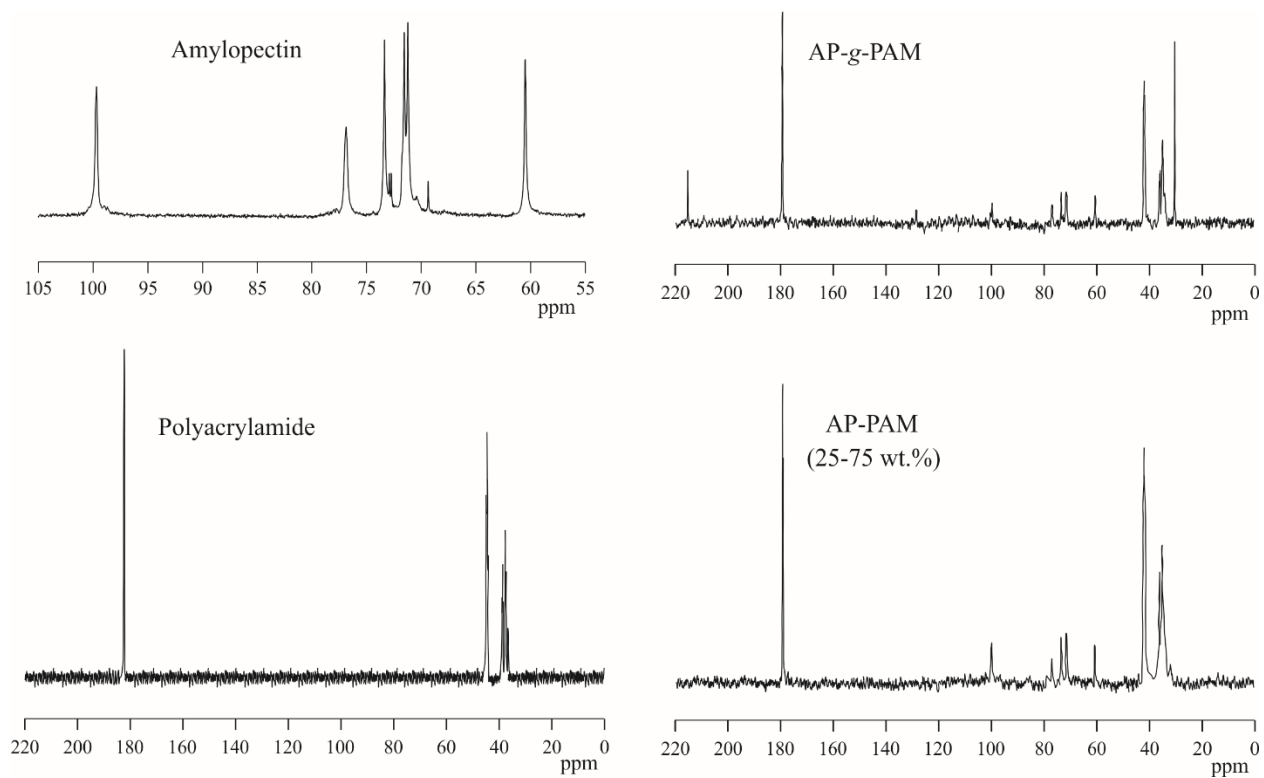


Figure 3.4. Carbon NMR chemical shifts of AP, PAM, AP-g-PAM, and AP-PAM.

3.2.3. Thermogravimetric Analysis (TGA)

Table 3.9 lists all the samples used for TGA. TGA measurements for weight loss versus temperature for three different AP-g-PAM samples in powder form are shown in Figure 3.5. Comparison of different AP-g-PAM grades showed that all samples had the same decomposition trend.

Table 3.9. TGA samples.

Sample	Explanation
AP	Commercial amylopectin
PAM	Commercial polyacrylamide (CP ₁)
AP-PAM	Amylopectin (25 wt.%) and polyacrylamide (75 wt.%) blend
AP-g-PAM	Unpurified amylopectin grafted polyacrylamide (unpurified G-6-2.5, G-8-3.5, and G-4-1.5)
P(AP-g-PAM)	Purified amylopectin grafted polyacrylamide (purified G-4-1.5)

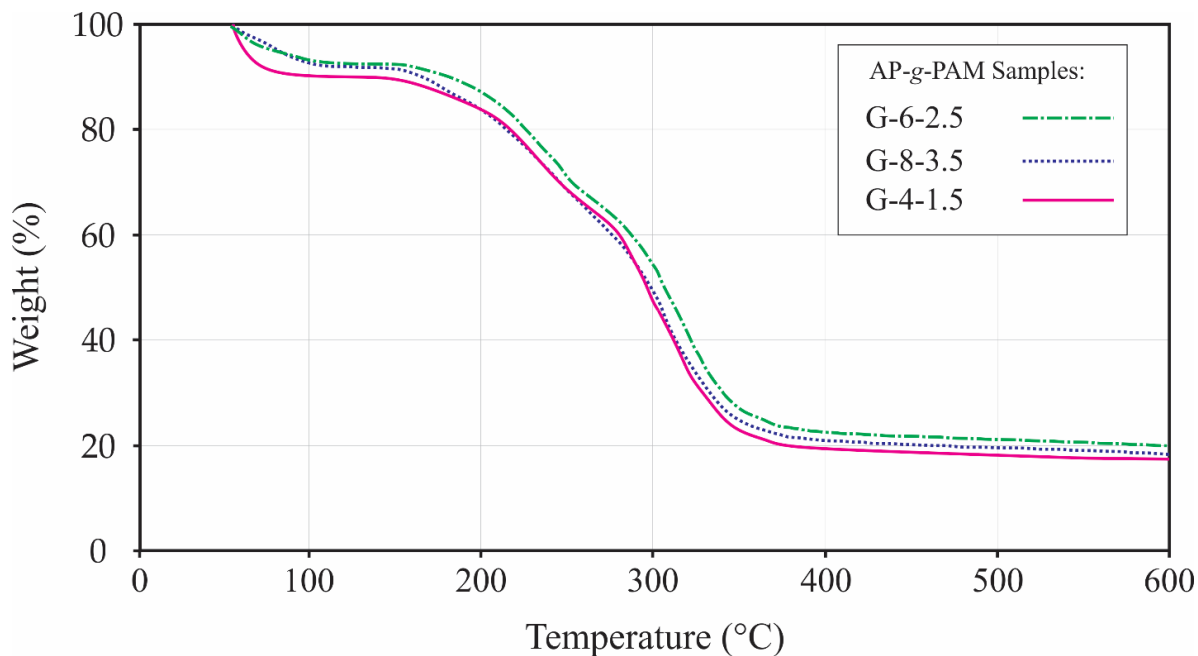


Figure 3.5. TGA weight loss versus temperature for three different AP-g-PAM samples.

Figure 3.6 shows TGA curves for AP, PAM, AP-g-PAM, P(AP-g-PAM) and AP-PAM samples. All samples were used in powder forms. The observed weight loss below 150 °C for all samples may be because of moisture loss. One single stage decomposition at around 250 °C was observed for the AP backbone, while PAM showed a multi-stage decomposition pattern.

The AP-g-PAM sample did not show the sharp weight loss observed at around 250 °C for AP, and its TGA profile also differed from that of PAM. This, alongside with the FTIR and NMR results, could confirm that both AP backbone and PAM chains were present in the sample. However, one could still think that it was only a physical mixture of AP and PAM, not a graft copolymer. To address this issue, the AP-PAM mixture with 25 wt. % of AP was analyzed by TGA. However, the AP-PAM physical mixture had a TGA profile that is substantially different from that of AP-g-PAM. This observation could confirm that the graft polymerization was successful, and that PAM chains were chemically grafted onto AP backbones.

The TGA weight loss for P(AP-g-PAM) followed the same trend for AP-g-PAM, but occurred at lower temperatures, perhaps because of the loss of the PAM chains. In fact, presence of impurities, PAM chains, in unpurified sample, AP-g-PAM, could make the degradation occur at higher temperature.

Although all the samples were in the powder form, the effect of polymer forms on TGA results should also be studied to make sure the difference in TGA decomposition trends is not from the difference in the form of polymers.

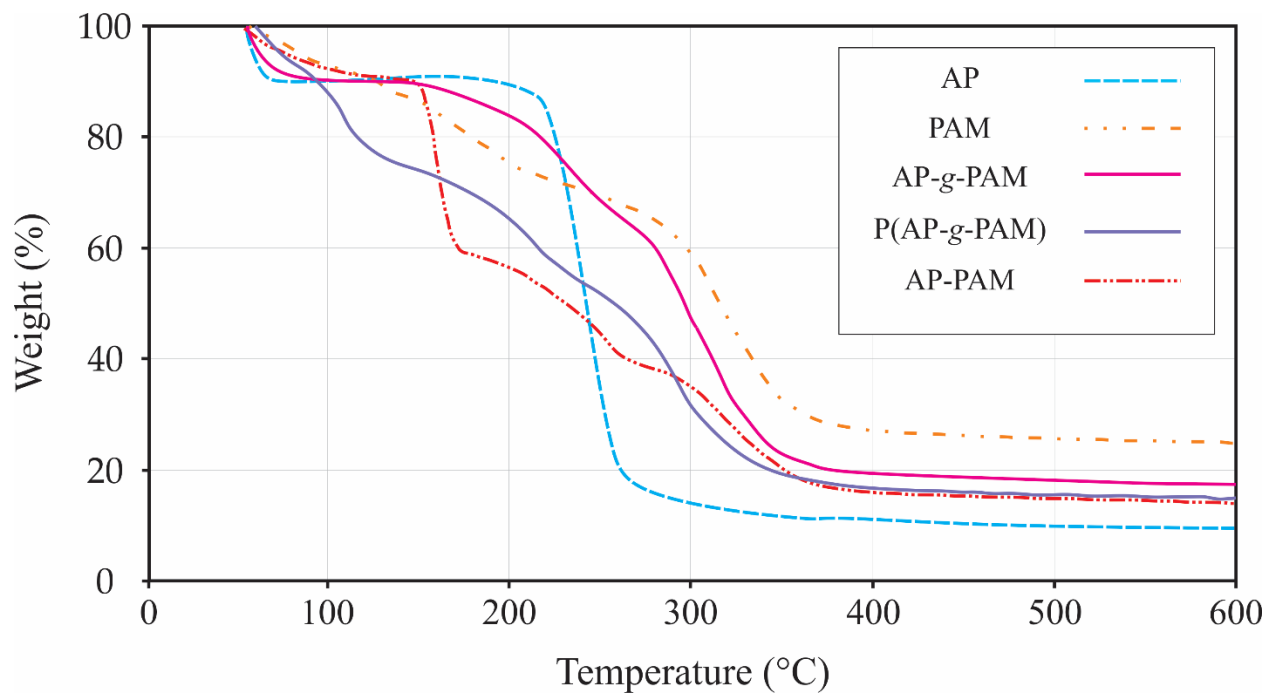


Figure 3.6. TGA weight loss versus temperature for AP, PAM, AP-g-PAM, P(AP-g-PAM), and AP-PAM.

3.2.4. Scanning Electron Microscopy (SEM)

Table 3.10 lists all the samples used to take SEM images. SEM images of AP and AP-g-PAM are shown in Figure 3.7. The left image shows that AP has granular morphology, while the right image shows the lace-like structure of AP-g-PAM.

Table 3.10. SEM samples.

Sample	Explanation
AP	Commercial amylopectin
PAM	Commercial polyacrylamide (CP ₁)
AP-PAM	Amylopectin and polyacrylamide blend
AP-g-PAM	Unpurified amylopectin grafted polyacrylamide (unpurified G-4-1.5)

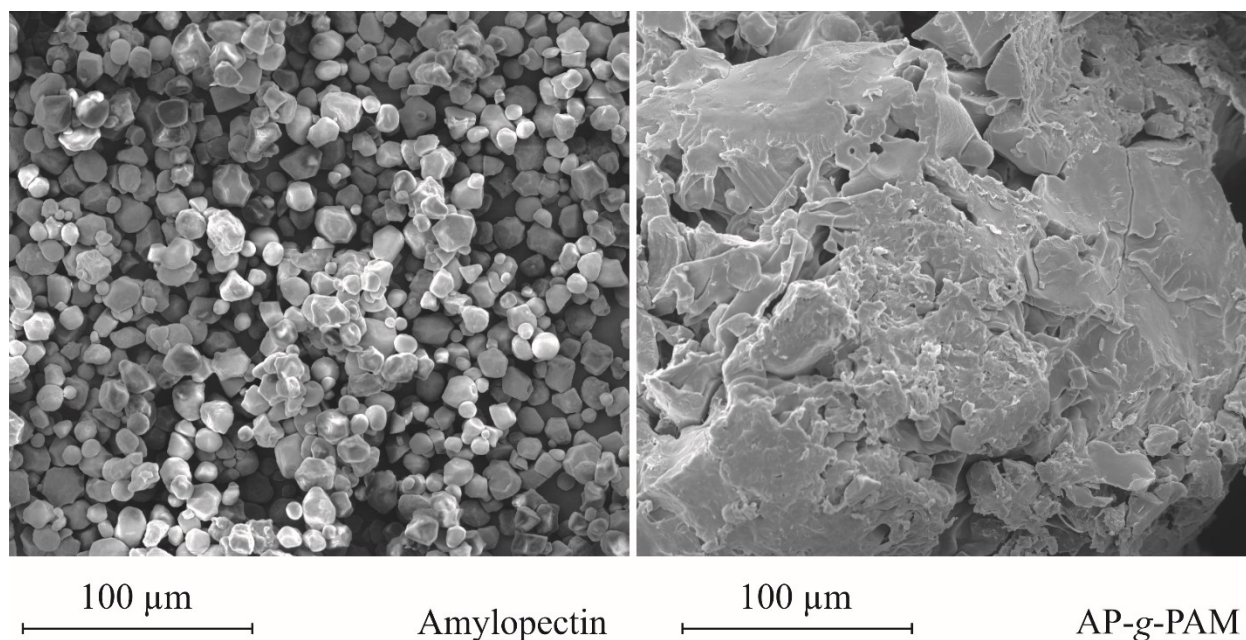


Figure 3.7. SEM images of AP (left) and AP-g-PAM (right).

To further study the morphology of grafted polymers, the SEM images of AP, PAM, and their mixture are shown in Figure 3.8. The top images show the AP and PAM mixture; as the size of PAM granules are bigger than AP, it was not possible to focus on both polymers at the same time: the focus of left image is on the AP granules, and the right image focused on the PAM granules.

The bottom images show AP and PAM separately at higher magnifications. The results showed that the structure of AP-g-PAM in Figure 3.7 resembles more that of PAM than AP, and it is certainly very different form the AP-PAM mixture.

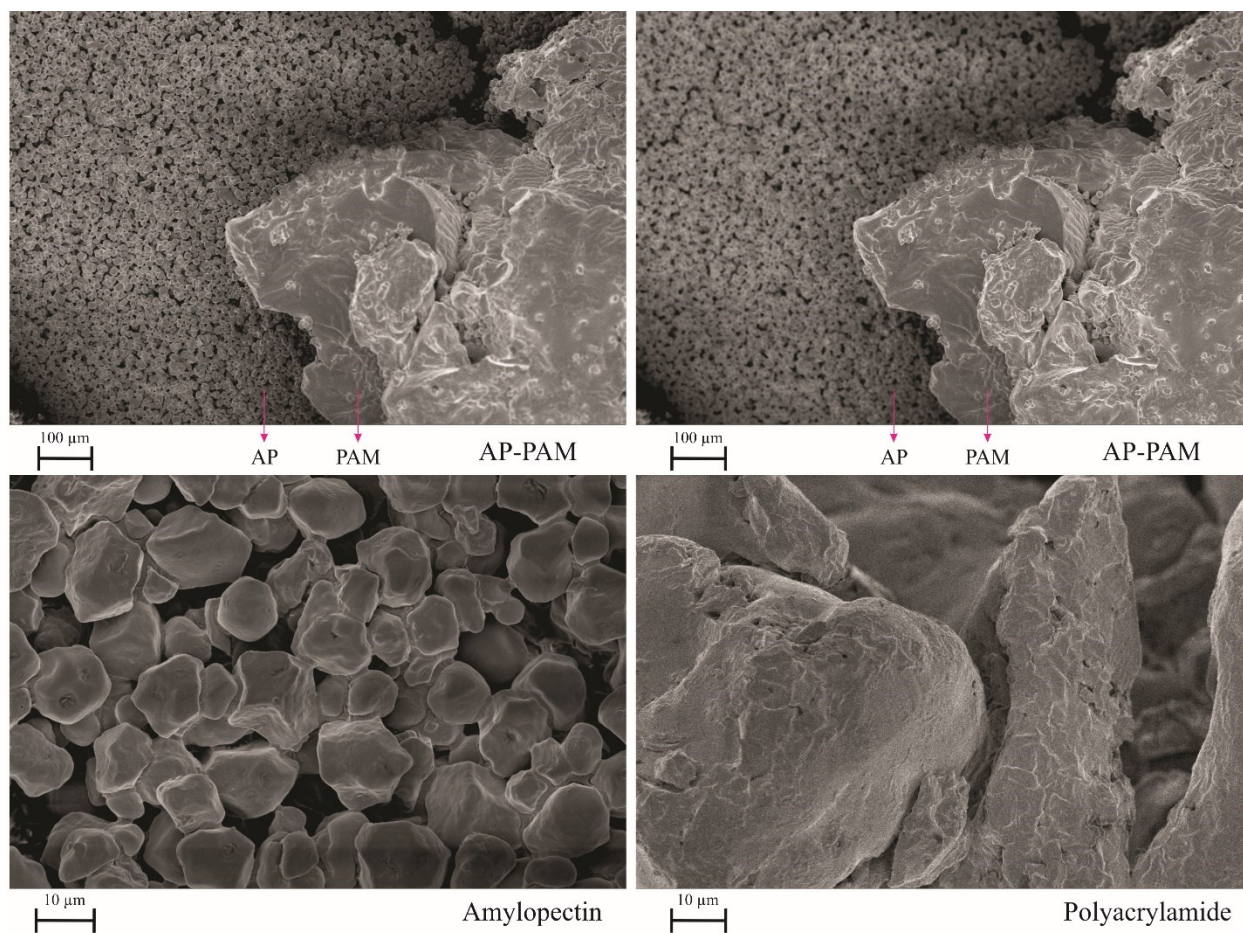


Figure 3.8. SEM images of AP-PAM, AP, and PAM.

3.3. MFT characterization

Moisture Analysis

Table 3.11 shows the water and solids weight percentage of the MFT sample used in this study. The solids content of the MFT was about 38 wt. %. This value was used to calculate the required amount of water for further dilution of MFT in flocculation tests.

Table 3.11. Moisture analysis of the MFT.

Component	Weight %
Water	~62
Solids	~38

Dean-Stark Analysis

The results of the Dean-Stark extraction are presented in Table 3.12. Because of the operational error, there is a slight difference between the moisture analysis and Dean-Stark extraction results.

Table 3.12. Dean-Stark analysis of the MFT.

Component	Weight %
Water	~60
Solids	~37
Bitumen	~3

Particle Size Distribution

Figure 3.9 shows the particle size distribution of MFT sample in both number and volume densities. The volume D_{50} of the sample is $13.9\ \mu\text{m}$, which means that 50 % of the particles volume is occupied by the particles with $13.9\ \mu\text{m}$ diameter or less. The number density curve shows that the number of finer particles are predominant to the extent that 50 % of the particles are $0.506\ \mu\text{m}$ or less in diameter.

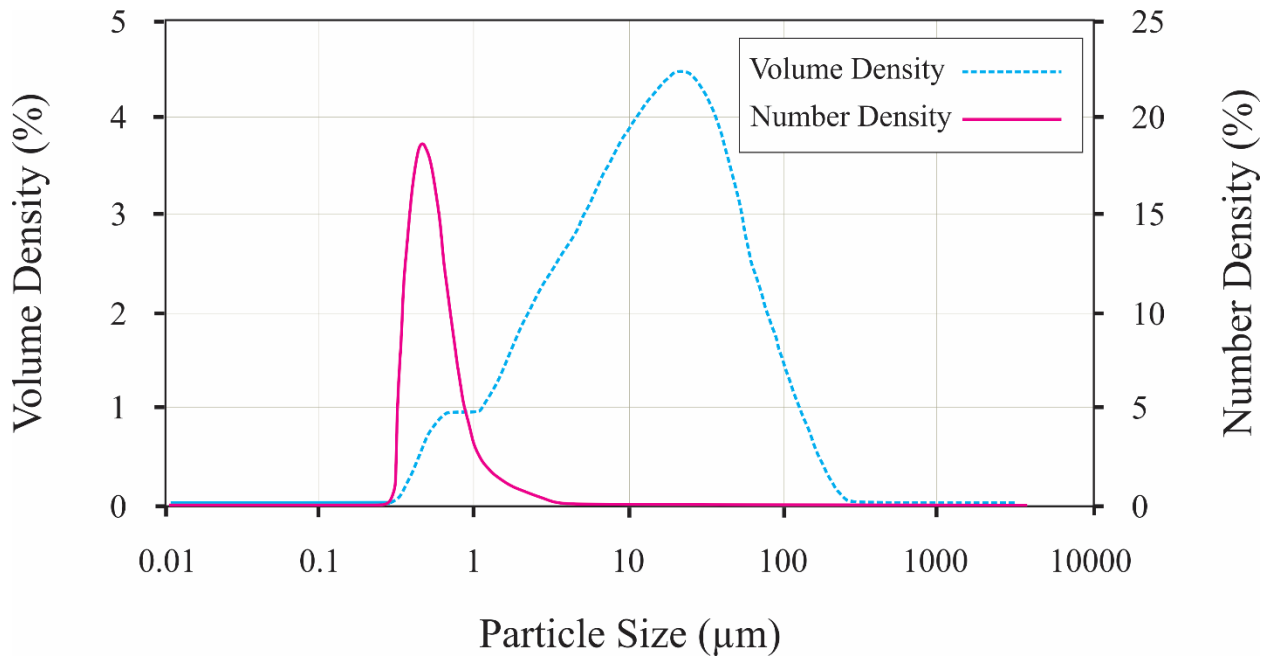


Figure 3.9. Particle size distribution (PSD) of the MFT.

Atomic Absorption Spectrophotometry (AAS)

Atomic absorption spectrophotometry has been performed to measure the ionic composition of MFT sample. Table 3.13 shows the concentration of sodium, calcium, potassium, and magnesium in undiluted MFT.

Table 3.13. Ion composition of the MFT.

Ion	Concentration (ppm)
Sodium (Na ⁺)	267.9
Calcium (Ca ²⁺)	22.5
Potassium (K ⁺)	21.0
Magnesium (Mg ²⁺)	11.5

3.4. Flocculation Tests

3.4.1. Flocculation Parameters and Reproducibility of Flocculation Tests

Based on their characteristics, polymers perform differently in flocculation tests, some of them form huge flocs, others make small flocs, some might be successful in capturing fine particles and clearing the water, while others might be able to form flocs with high solids contents. All these metrics should be considered when evaluating a flocculant. One polymer might be superior in one performance metric while performing poorly in others.

Turbidity and solids content were considered the main determining metrics in this investigation because the main flocculation goal is to separate the fine particles from water (low turbidity of supernatant) and create dense flocs (high solids content of sediment). Turbidity of DI water was measured to be 0.24 NTU, and the turbidities of MFT samples with 0.5 wt.% or more solids were beyond the detection limits of the instrument, with values of 10,000 NTU (Appendix A). Supernatants with turbidities below 250 NTU appear totally clear to the naked eye.

Figure 3.10 analyzes the typical repeatability of these measurements. H-2.5 is a PAM homopolymer, and G-4-2.5 is one of the AP-g-PAM samples. H-2.5₁, H-2.5₂, G-4-2.5₁, and G-4-2.5₂ show results for each polymer and their replicates. The highest errors were observed for CST measurements, especially for the CST of sediments. That is because of two main reasons. First, because the flocs were large, it was difficult to sample them homogeneously for CST measurements. Second, the water content of the sediments might be very low, making it hard to measure CST accurately. In such cases, it is better to judge the polymer performance based on the solids content of the sediments.

Except for samples G-4-2.5₁ and G-4-2.5₂ dosed at 6,000 ppm, all the turbidity results were reproducible. This difference might be attributed to floc breakage, leading to fine formation in the G-4-2.5₂ case. Poor reproducibility was also observed for solids content of G-4-2.5₁ and G-4-2.5₂ dosed at 4,000 ppm. As flocs were small at 4,000 ppm, the sediments were watery, which made it hard to separate the sediment from the supernatant.

The overall flocculation performance of G-4-2.5 and H-2.5 were approximately the same, likely because of the low weight percentage of AP used in polymerization of G-4-2.5, 16.45 wt.%.

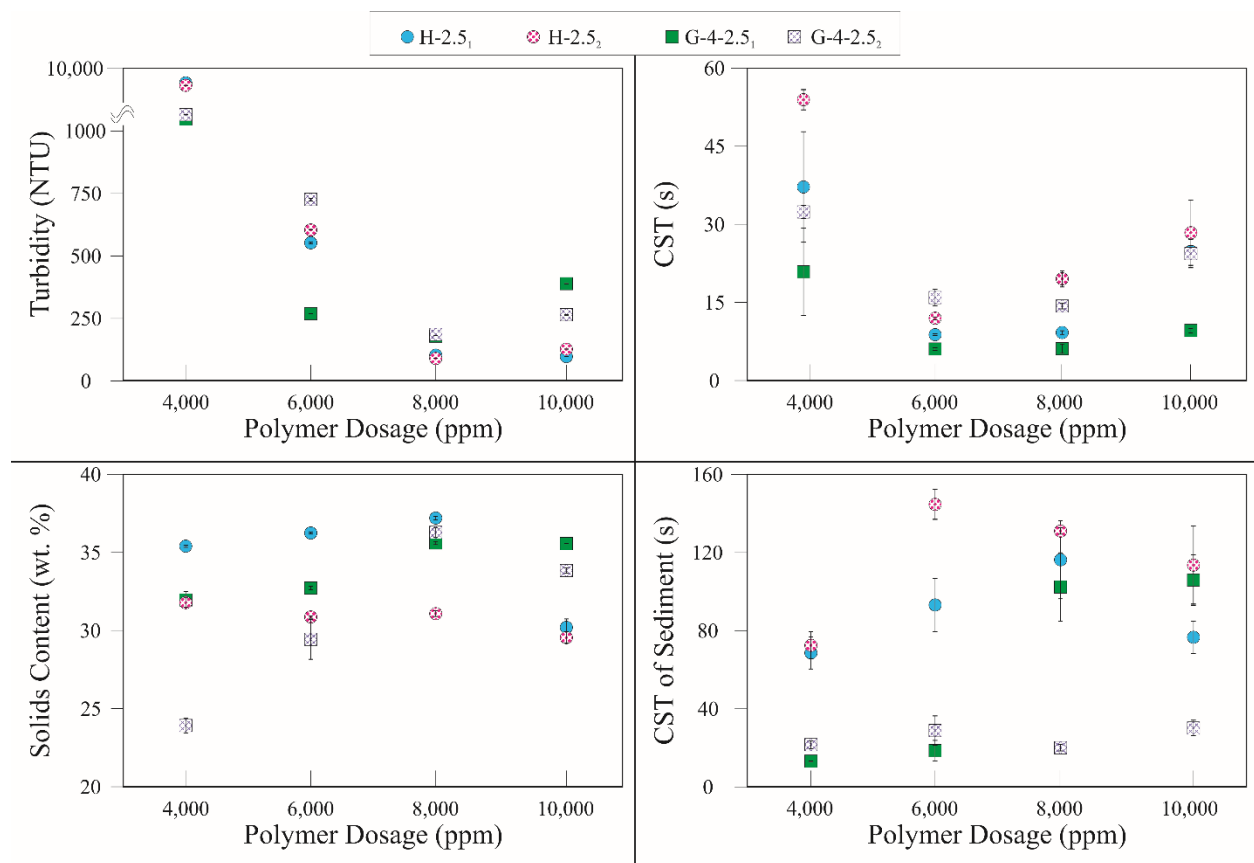


Figure 3.10. Reproducibility of flocculation and dewatering results.

3.4.2. Amylopectin Flocculation

Amylopectin was used as a flocculant for MFT, and the results were compared with a sample of AP-g-PAM, G-4-2.5, one PAM sample, H-2.5, and the blend of AP and PAM, AP-H-2.5. The AP weight percentage in AP-H-2.5 sample was kept constant at 16.5 wt. % at all the dosages. This is the same as AP weight percentage used in polymerization of G-4-2.5.

Figure 3.11 shows pictures of the MFT flocculated with AP, H-2.5, AP-H-2.5, and G-4-2.5 after 24 h. Flocculation and dewatering performance parameters are plotted in Figure 3.12. AP did not flocculate MFT well, and the supernatants were not clear even at higher dosages. H-2.5, AP-H-2.5, and G-4-2.5 were not efficient at 4,000 ppm, however, their performance got better at 6,000 ppm and higher dosages. Considering the 6,000 ppm samples as optimum dosage, the supernatant was clearest for G-4-2.5. Turbidities also confirmed this as the turbidity of AP-g-PAM, 264 NTU, was lower than PAM, 553 NTU, and AP-PAM, 594 NTU, samples.

The results showed that AP itself would not be a good flocculant to flocculate diluted MFT that might be because of its low molecular weight which was measured to be approximately 0.5 MDa. Moreover, the overall flocculation performance of G-4-2.5 was like H-2.5. This might be because of low weight percentage of AP used in polymerization of G-4-2.5.

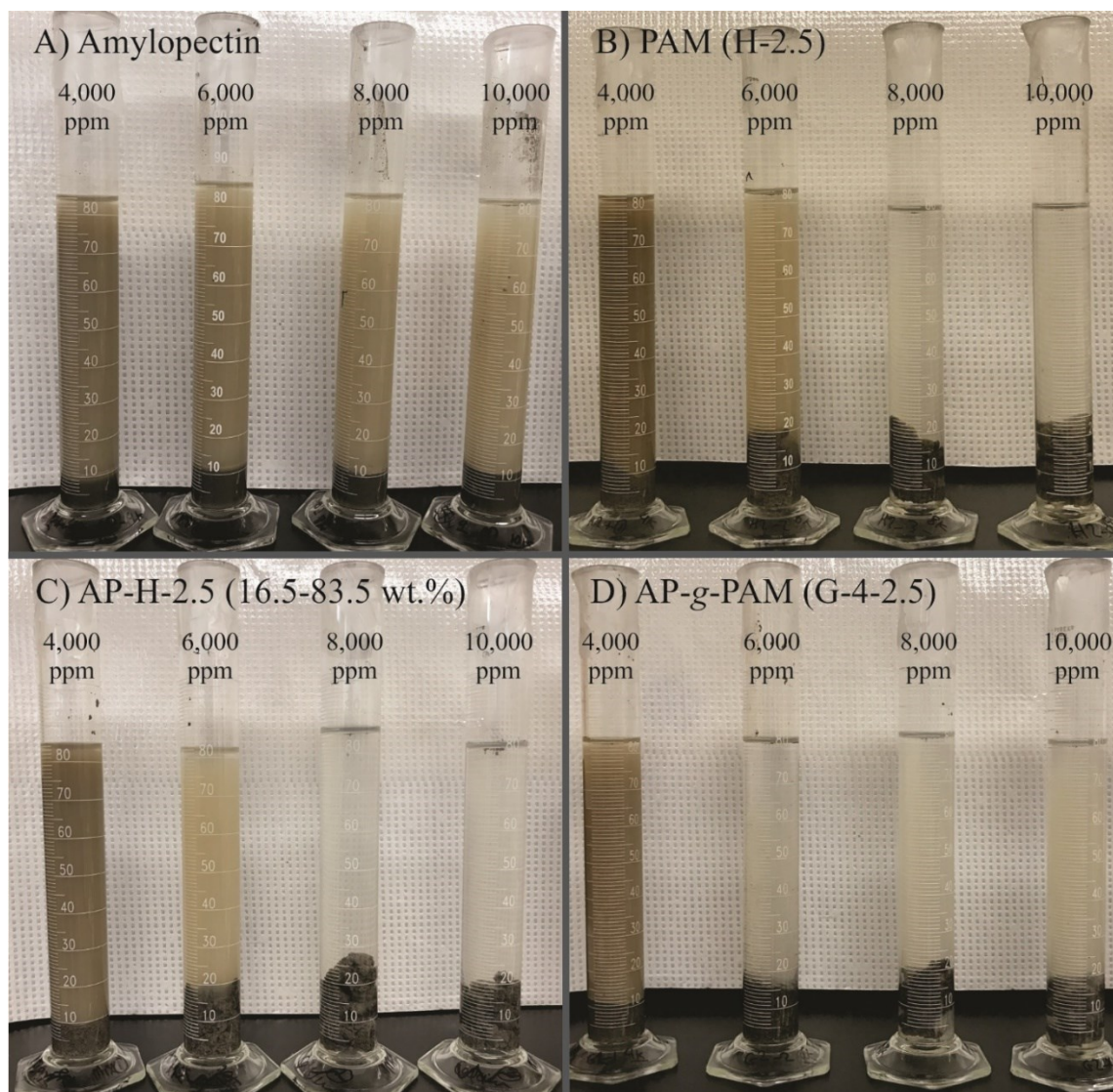


Figure 3.11. Flocculated MFT by AP, H-2.5, AP-H-2.5, and G-4-2.5 after 24 h at different polymer dosages.

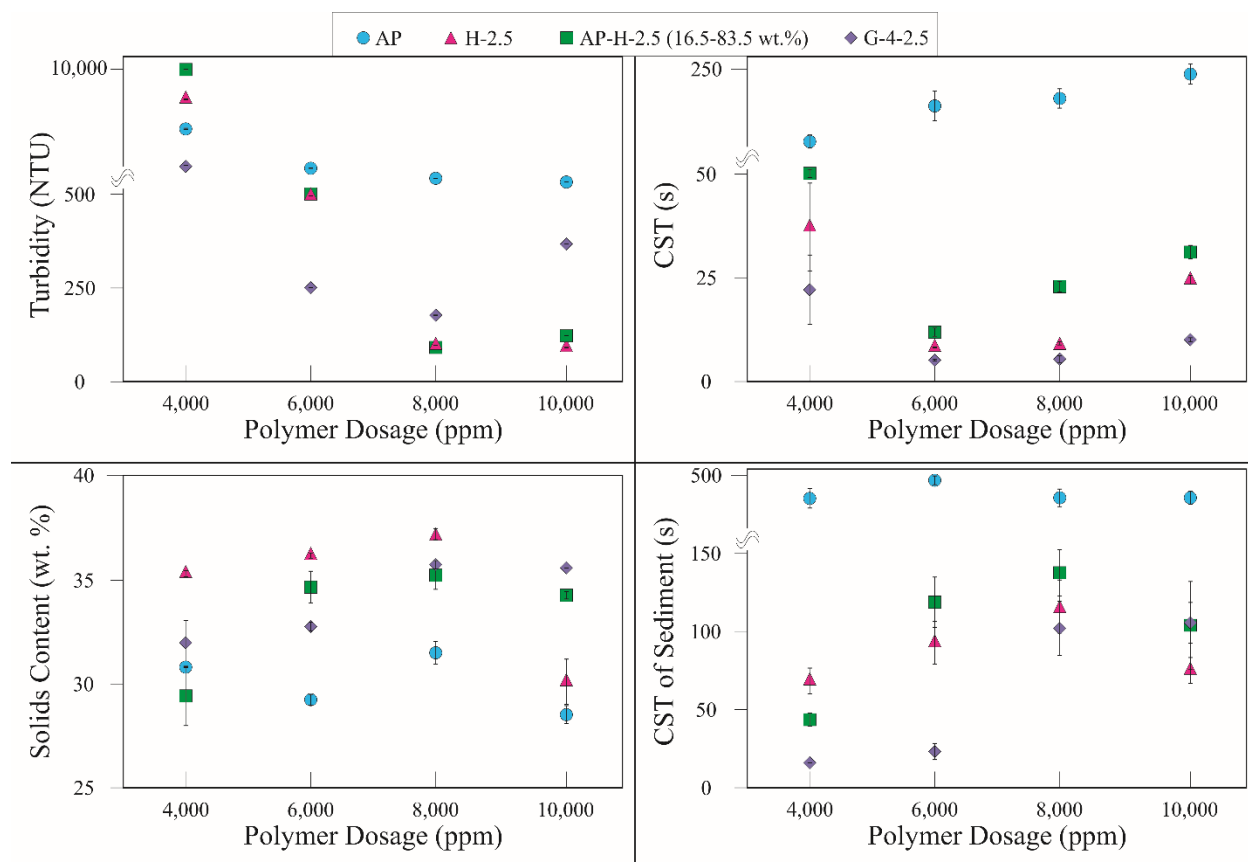


Figure 3.12. Flocculation results of AP, H-2.5, AP-H-2.5, and G-4-2.5.

3.4.3. AP-g-PAM Flocculation Performance

Figure 3.13 shows the flocculation results with G-4-0.25, G-4-2.5, G-4-0.5, and G-4-1.5. In polymerizations of G-4-0.25 and G-4-2.5, the same mass of AP and AM were used, however, the initiator concentration used in polymerization of G-4-0.25 was 10 times higher than that of G-4-2.5 in G-4-2.5 polymerization. The number of active sites on the AP could increase by increase in initiator concentration, therefore, more grafts with shorter chains could form in G-4-0.25 as the

number of monomers are the same in either cases. Long grafts of PAM are likely to flocculate more fine particles as they are long enough to extend in the solution. So, before the flocculation we expected to get better flocculation results with G-4-2.5 compared to G-4-0.25.

Supernatant turbidity of G-4-2.5 at 6,000 was significantly lower than that of G-4-0.25. This shows that G-4-2.5 is much more efficient at lower dosages that might be because of longer chains of PAM attached to AP. Solids contents of G-4-2.5 were also higher than that of G-4-0.25, which confirms the better flocculation ability of G-4-2.5. CST of sediment at 8,000 and 10,000 ppm are too high for G-4-2.5 which might be because of high solid contents of sediment and a very low content of water in the flocs to be released. However, the CST of sediment at 6,000 is still reasonable (20 s).

The effect of monomer concentration could be studied by comparing the flocculation performance of G-4-2.5, G-4-0.5, and G-4-1.5. The amount of AP and CAN used in the polymerizations of these polymers were the same, however, the concentrations of AM were 0.1, 0.3, and 0.5 M for G-4-0.5, G-4-1.5, and G-4-2.5, respectively. Increase in monomer concentration may increase the molecular weight and length of PAM grafts, and result in more efficient flocculations.

G-4-0.5 did not show good results in turbidity, solids contents, and CSTs before 8,000 ppm as predicted because the concentration of monomer was not high enough to produce high molecular weight polymer. Performance of G-4-2.5 was also better than G-4-1.5 as lower turbidity was obtained at 6,000 while other parameters were fairly similar for either polymers. As expected, G-4-2.5 had the best performance among these polymers, with higher solids contents and lower turbidities and CSTs, due to higher monomer to initiator ratio.

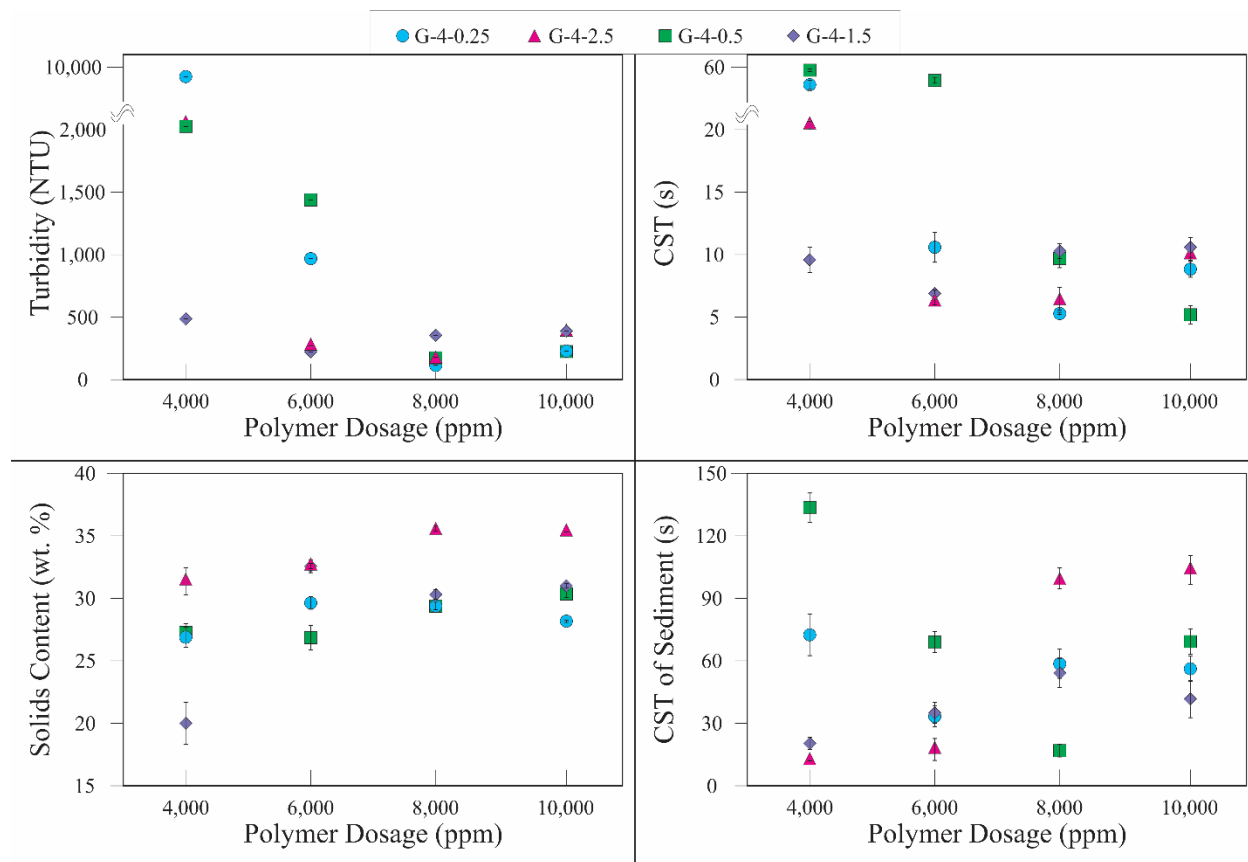


Figure 3.13. Flocculation performance of G-4-0.25, G-4-2.5, G-4-0.5, and G-4-1.5.

It was shown that monomer and initiator concentrations had significant effects on flocculation performance of the polymers. However, the amount of AP used in polymerization may also have effect in molecular weight and flocculation performance of the polymers. So, in another set of flocculations, the flocculation abilities of G-4-2.5, G-6-2.5, and G-8-2.5 were compared. The initiator and monomer concentrations were similar in their polymerizations, however, the amount of AP increased in G-6-2.5 and G-8-2.5 compared to G-4-2.5. As the ratio of the monomer to initiator were the same for these polymers, the length and numbers of the PAM grafts were expected to be the same. However, increase in AP used in polymerization may increase the average

distance between PAM grafts; By increase in the AP amount, the ratio of initiator to backbone decreases which could result in forming less numbers of grafts on each AP backbone.

Figure 3.14 shows the flocculation results of G-4-2.5, G-6-2.5, and G-8-2.5. Compared to G-4-2.5, flocculation performance of G-6-2.5 significantly improved by increasing AP. The best turbidity obtained for G-6-2.5 was 125 NTU at 4,000 ppm, while at the same dosage the turbidity of G-4-2.5 was above 2,700 NTU. The solids content and CST of the whole suspension were also good at 4,000 ppm for G-6-2.5. However, the CST of sediment was too high that might be because of lack of water in the sediment. The flocculation results of G-8-2.5 showed that further increase in AP used in a polymerization could deteriorate the polymer's flocculation ability, and there could be an optimum initiator to AP ratio for graft polymers. These results show that the change in AP during polymerization step could have a significant effect on the flocculation performance of the polymer.

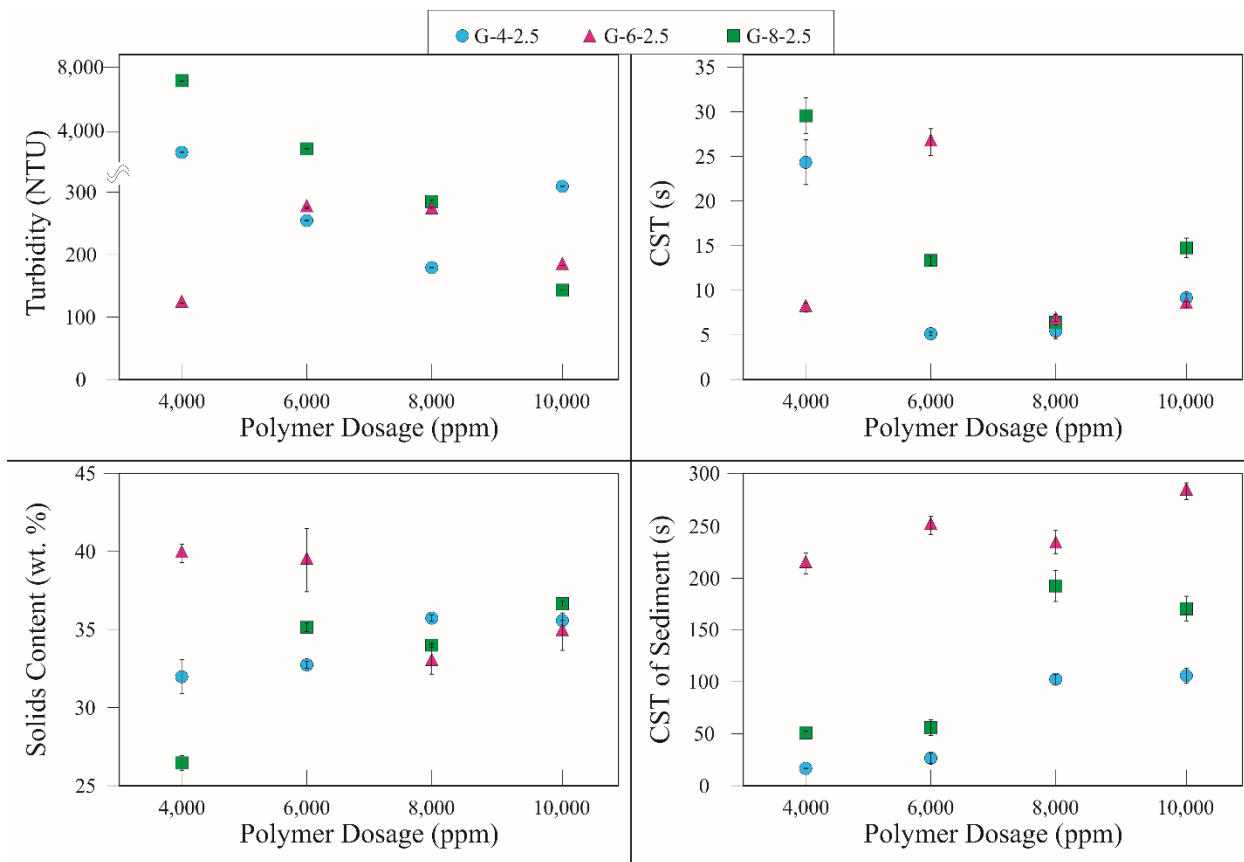


Figure 3.14. Flocculation performance of G-4-2.5, G-6-2.5, and G-8-2.5.

Figure 3.15 shows the flocculation results of G-6-3.5, G-6-2.5, G-8-3.5, and G-8-5. As the flocculation performance of G-6-2.5 was promising, polymer G-6-3.5 was synthesized to see if further increase in monomer concentration could improve the flocculation performance. So, the monomer concentration was increased from 0.5 to 0.7 M for polymerization of G-6-3.5. The flocculation performance of G-6-3.5 showed that increase in AM concentration could improve the flocculating efficiency of polymer, however, as the improvement was not so much, one could prefer to use G-6-2.5 as it performs similar to G-6-3.5 but with less amount of monomer used. This might decrease the total operational cost.

Polymer G-8-3.5 was also prepared with the same monomer to initiator ratio of that of the G-6-3.5 (3500). However, the AP used in polymerization was increased to study the effect of AP fraction at this monomer to initiator ratio. As the AP to initiator ratio increases, the numbers of PAM grafts on a single backbone may decrease, so, the optimum dosage of G-8-3.5, 8,000 ppm, is higher than that of G-6-3.5, 4,000 ppm. It is interesting that the turbidity of G-8-3.5 at 8,000 ppm is the lowest among all the polymers. This could show that the more space between long PAM grafts on the AP backbones could result in better reachability of the chains by fine particles.

The monomer to initiator ratio was increased to 5,000 for G-8-5 by increasing the monomer concentration. Compared to G-8-3.5, the same amount of initiator and AP were used, so, the flocculation performance was expected to become superior for G-8-5 due to longer PAM chains. Although the turbidities were lower for G-8-5 at low dosages (4,000 and 6,000 ppm), the solids content of sediments were too low which might be because of presence of too much hydrophilic PAM chains in the graft polymers. This shows that the ratio of monomer to AP is also important as it changes the hydrophilicity of the graft polymer. The weight percentages of AP were approximately same for G-6-3.5, 16.73, and G-8-5, 16.45 wt.%, however, the length of the chains in G-8-5 might be very long that traps water molecules, deteriorating the dewaterability of the flocs.

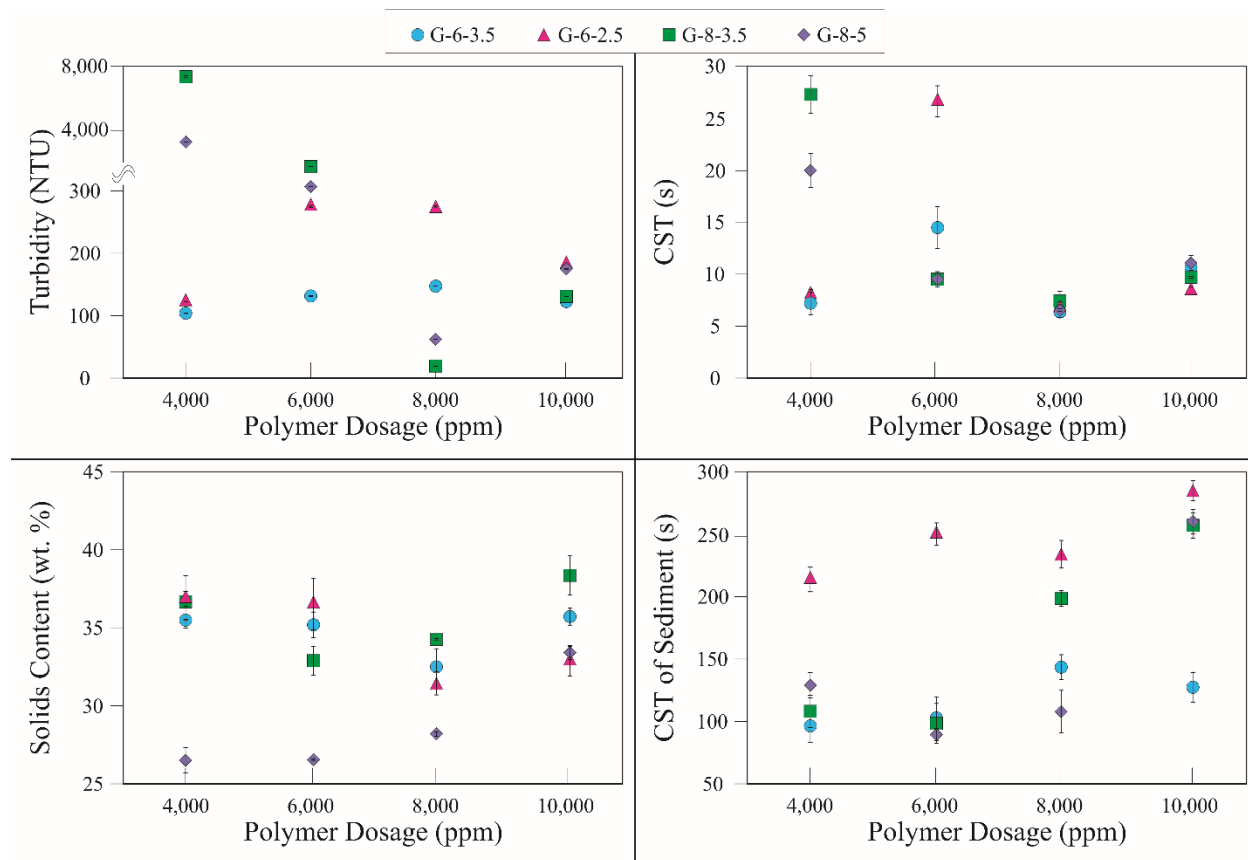


Figure 3.15. Flocculation performance of G-6-3.5, G-6-2.5, G-8-3.5, and G-8-5.

Flocculation performance of the best polymer, G-6-3.5, was compared with two commercial polymers, CP₁ and CP₂, in Figure 3.16. Compared to CP₁, CP₂ showed better efficiency to capture fine particles, resulting in lower turbidities at all dosages. However, because the molecular weight of CP₂ is higher, the PAM chains are longer and can entrap water in the flocs so that it is harder for the flocs to release the water. That is why the CSTs and solids content of CP₂ seemed to be inferior compared to CP₁.

Although CP₁ did not show good performance at 4,000 ppm, CP₂ and G-6-3.5 had their best performance at 4,000 ppm, showing that both CP₂ and G-6-3.5 are efficient flocculants at lower

dosages. This might be because of higher molecular weight of CP₂ and G-6-3.5 compared to CP₁. At 4,000 ppm, although the turbidity of CP₂, 40 NTU, is lower than that of G-6-3.5, 104, the CSTs and solids contents of G-6-3.5 are superior. This shows that G-6-3.5 is able to capture fine particles and release the water faster. The most interesting aspect of G-6-3.5 compared to CP₁ and CP₂ is that it produced sediments with higher solid contents at all the dosages. This shows that presence of AP in AP-g-PAMs can result in better dewaterability of the flocculants.

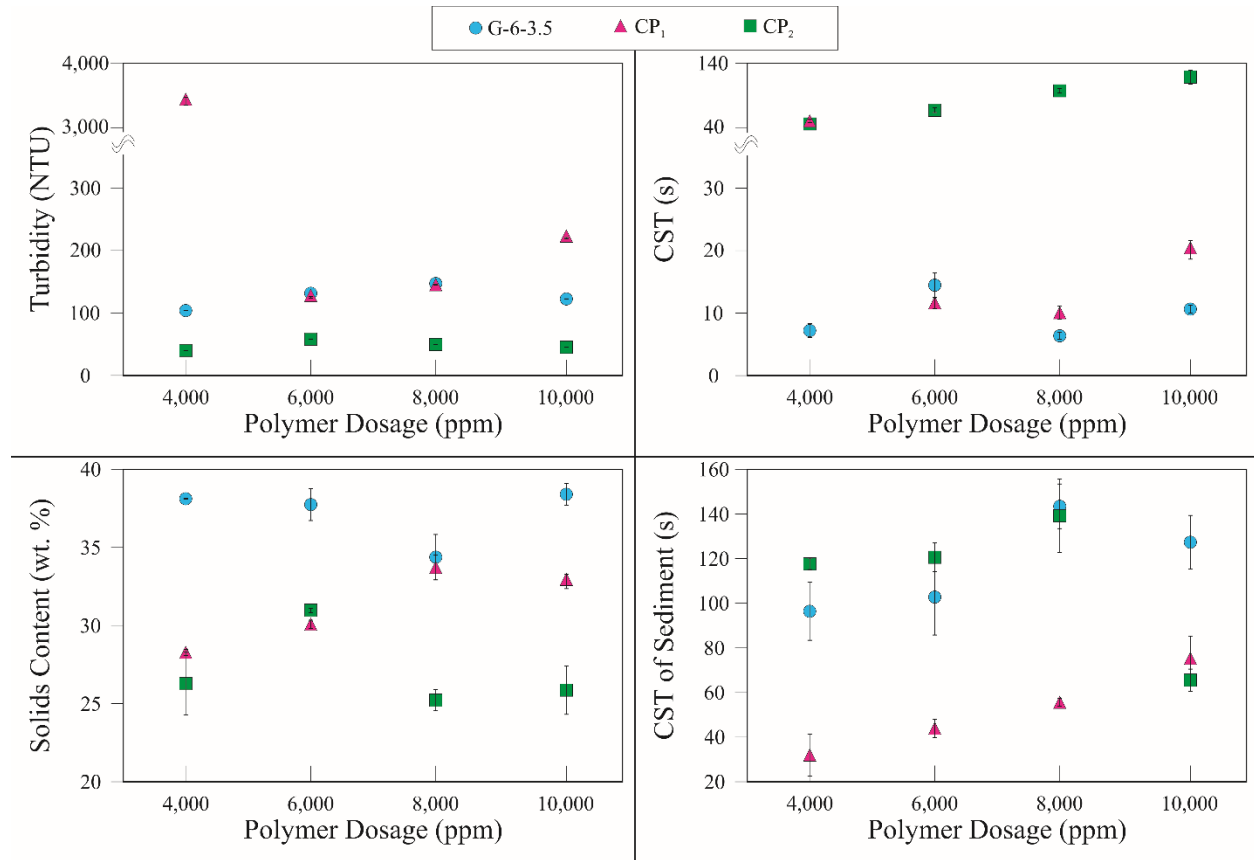


Figure 3.16. Flocculation results of G-6-3.5, CP₁, and CP₂.

3.4.4. Sieve Test

Figures 3.17, 3.18, and 3.19 show the solids contents of flocculated MFT versus time at 6,000, 8,000, and 10,000 ppm, respectively. Sieve tests were performed to compare the natural abilities of the flocs to release water right after flocculation, after 30 min, and after 1 h. MFT suspensions were also diluted to 10 wt.% solids to test the flocculation abilities of polymers at higher solids content of MFT. The performances of grafted polymers (G-6-2.5, G-6-3.5, G-8-2.5, G-8-3.5, and G-8-5) were compared to those of commercial and synthesized PAMs (CP₁, CP₂, H-3.5, and H-5).

At 6,000 and 8,000 ppm, (Figures 3.17 and 3.18), CP₂ and H-5 showed lower solids contents compared to all the AP-g-PAM samples. CP₂ and H-5 have higher molecular weights compared to CP₁ and H-3.5. So, it shows that despite the fact that the high molecular weight PAMs are better flocculants in capturing the fine particles, they produce flocs with lower solid contents due to high hydrophilicity of PAM chains. So, use of AP in the structure of AP-g-PAM might be a good solution to this problem to have high molecular weight polymers that make flocs with better dewaterability performance. However, at 10,000 ppm, (Figure 3.19), the solids contents of AP-g-PAM samples decreased compared to lower dosages which might be because of over dosing effect.

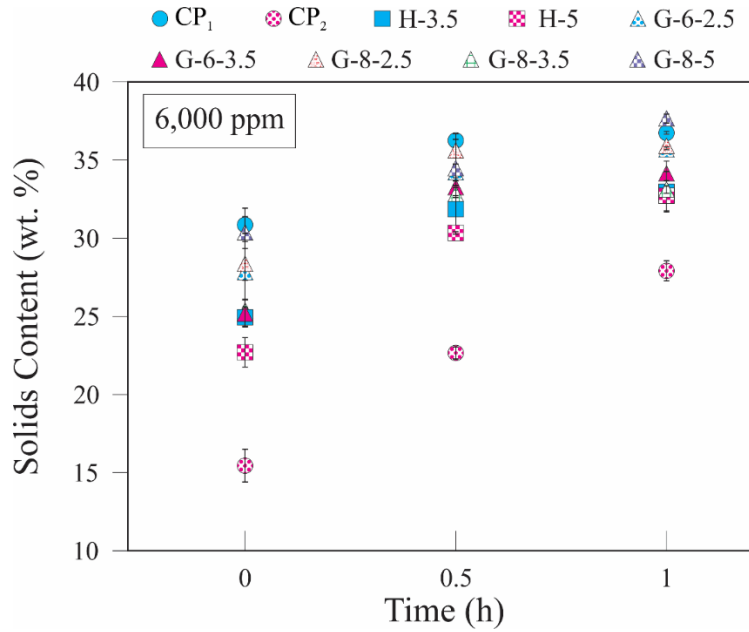


Figure 3.17. Solids content of flocculated MFT for sieve test versus time for CP₁, CP₂, H-3.5, H-5, G-6-2.5, G-6-3.5, G-8-2.5, G-8-3.5, and G-8-5 at 6,000 ppm.

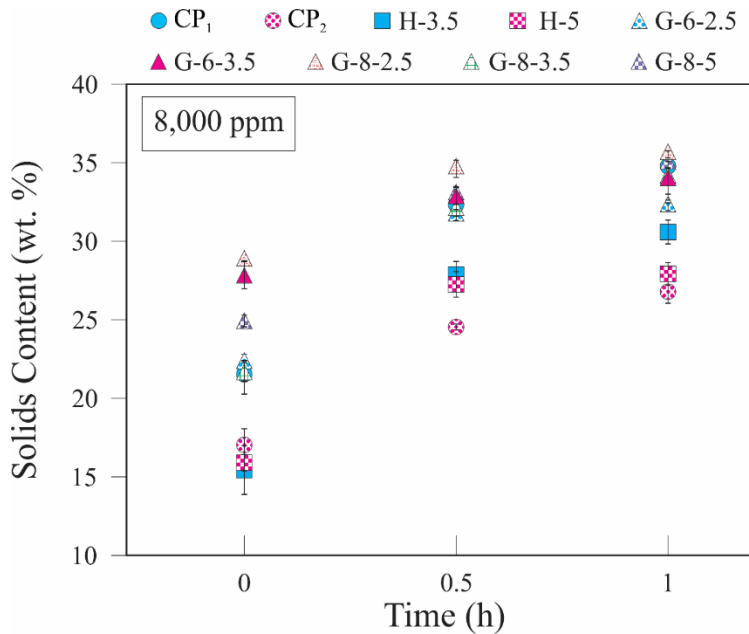


Figure 3.18. Solids content of flocculated MFT for sieve test versus time for CP₁, CP₂, H-3.5, H-5, G-6-2.5, G-6-3.5, G-8-2.5, G-8-3.5, and G-8-5 at 8,000 ppm.

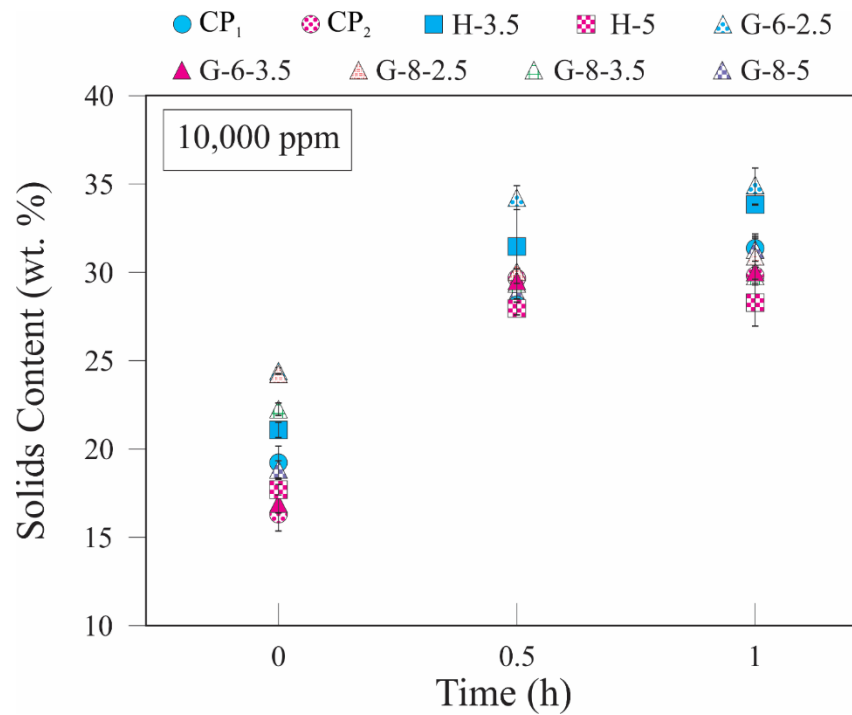


Figure 3.19. Solids content of flocculated MFT for sieve test versus time for CP₁, CP₂, H-3.5, H-5, G-6-2.5, G-6-3.5, G-8-2.5, G-8-3.5, and G-8-5 at 10,000 ppm.

3.5. References

1. Pavia DL, Lampman GM, Kriz GS. Chapter 2. Infrared Spectroscopy. In: Introduction to Spectroscopy: A Guide for Students of Organic Chemistry. Fort Worth: Harcourt College Publishers, 2001.
2. Lin-Vien D, Colthup NB, Fateley WG, Grasselli JG. Appendix 3 - A Summary of Characteristic Raman and Infrared Frequencies. In: The Handbook of Infrared and Raman Characteristic Frequencies of Organic Molecules. San Diego: Academic Press, 1991. p. 477-490.
3. Pavia DL, Lampman GM, Kriz GS. Chapter 6. Nuclear Magnetic Resonance Spectroscopy. Part Four: Other Topics in One-Dimensional NMR. In: Introduction to Spectroscopy: A Guide for Students of Organic Chemistry. Fort Worth: Harcourt College Publishers, 2001.
4. Al-Sabagh AM, Kandile NG, El-Ghazawy RA, Noor El-Din MR, El-sharaky EA. Synthesis and characterization of high molecular weight hydrophobically modified polyacrylamide nanolatexes using novel nonionic polymerizable surfactants. Egyptian Journal of Petroleum 2013;22(4):531-538.
5. Sasmal D, Singh R, Tripathy T. Synthesis and flocculation characteristics of a novel biodegradable flocculating agent amylopectin-g-poly (acrylamide-co-N-methylacrylamide). Colloids Surf Physicochem Eng Aspects 2015;482:575-584.
6. Inoue Y, Fukutomi T, Chujo R. Carbon-13 NMR analysis of the tacticity of polyacrylamide. Polym J 1983;15(1):103-105.

7. Mora-Gutierrez A, Baianu IC. Carbon-13 nuclear magnetic resonance studies of chemically modified waxy maize starch, corn syrups, and maltodextrins. Comparisons with potato starch and potato maltodextrins. *J Agric Food Chem* 1991;39(6):1057-1062.
8. Falk H, Stanek M. Two-dimensional ^1H and ^{13}C NMR spectroscopy and the structural aspects of amylose and amylopectin. *Monatshefte fur Chemie / Chemical Monthly* 1997;128(8):777-784.
9. Paris M, Bizot H, Emery J, Buzaré JY, Buléon A. Crystallinity and structuring role of water in native and recrystallized starches by ^{13}C CP-MAS NMR spectroscopy. *Carbohydrate Polymers* 1999;39(4):327-339.
10. Dragunski D, Pawlicka A. Preparation and characterization of starch grafted with toluene poly(propylene oxide) diisocyanate. *Materials Research* 2001;4(2):77-81.
11. Pavia DL, Lampman GM, Kriz GS. Chapter 3. Nuclear Magnetic Resonance Spectroscopy. Part One: Basic Concepts. In: *Introduction to Spectroscopy: A Guide for Students of Organic Chemistry*. Fort Worth: Harcourt College Publishers, 2001.

Chapter 4: Conclusions and Future Works

Different grades of AP-g-PAM flocculants were synthesized and used to flocculate diluted MFT in jar tests (5 wt.% solids) and sieve tests (10 wt.% solids). FTIR, NMR, TGA, and SEM tests were used to characterize AP-g-PAM samples and the results were compared with those of AP, PAM, and their mixture, AP-PAM.

In FTIR and NMR results, AP-g-PAM showed characteristics of both AP and PAM. There was not any discernible difference between AP-g-PAM and AP-PAM. However, a significant difference between AP-g-PAM and AP-PAM was observed in TGA results. SEM results also showed that the AP-PAM morphology is completely different than AP-g-PAM as AP and PAM can be distinguished in their mixture based on their different sizes.

AP itself did not show good performance in flocculation of MFT because of having low molecular weight. However, it was shown that the AP-g-PAM samples could be more efficient to form flocs with higher dewaterabilities and solids contents. It was shown that monomer to initiator ratio and AP fraction affect the performance of AP-g-PAM samples to flocculate MFT.

As AP-g-PAM is not completely soluble in water, its application as a flocculant might be limited. Dissolving AP-g-PAM in water does not create a very clear solution. That is why AP-g-PAM samples could not be used to measure their molecular weight by gel permeation chromatography (GPC) or light scattering (LS).

AP could be replaced by natural polymers that have higher molecular weight and show better flocculation abilities such as hydroxypropyl methylcellulose (HPMC) in future works. It was also shown that AP grafted with neutral PAM is an effective flocculant only at polymer dosages higher than 4,000 ppm. Therefore, charged polymers graft such as hydrolyzed poly(methyl acrylate) (H-

PMA) that are effective at lower polymer dosages can be used to increase the efficiency of graft polymers. Amylopectin grafted hydrolyzed poly(methyl acrylate) (AP-g-H-PMA) and hydroxypropyl methylcellulose grafted polyacrylamide (HPMC-g-PAM) were synthesized and their flocculation performance will be compared to AP-g-PAM in our future works.

Bibliography

Ahuja S. Chapter 1. Overview: Water Reclamation and Sustainability. In: Ahuja S, editor. Water Reclamation and Sustainability. Boston: Elsevier, 2014. p. 1-18.

Alberta Energy Regulator (<http://www.aer.ca>).

Al-Sabagh AM, Kandile NG, El-Ghazawy RA, Noor El-Din MR, El-sharaky EA. Synthesis and characterization of high molecular weight hydrophobically modified polyacrylamide nanolatexes using novel nonionic polymerizable surfactants. *Egyptian Journal of Petroleum* 2013;22(4):531-538.

Beier N, Wilson W, Dunmola A, Segó D. Impact of flocculation-based dewatering on the shear strength of oil sands fine tailings. *Canadian Geotechnical Journal* 2013;50(9):1001-1007.

BGC Engineering Inc., 2010. Oil Sands Tailings Technology Review. Oil Sands Research and Information Network, University of Alberta, School of Energy and the Environment, Edmonton, Alberta. OSRIN Report No. TR-1. 136 pp.

Bolto B, Gregory J. Organic polyelectrolytes in water treatment. *Water Research* 2007;41(11):2301-2324.

Bonilla-Cruz J, Dehonor M, Saldívar-Guerra E, González-Montiel A. Chapter 10. Polymer Modification: Functionalization and Grafting. In: *Handbook of Polymer Synthesis, Characterization, and Processing*. : John Wiley & Sons, Inc., 2013. p. 205-223.

Botha L, Soares JBP. The Influence of Tailings Composition on Flocculation. *Can J Chem Eng* 2015;93(9):1514-1523.

Bratby J. Chapter 1. Introduction. In: *Coagulation and Flocculation in Water and Wastewater Treatment* (2nd Edition). London, UK: IWA Publishing, 2006. p. 1-8.

Bratby J. Chapter 2. Colloids and interfaces. In: *Coagulation and Flocculation in Water and Wastewater Treatment*. London, UK: IWA Publishing, 2006. p. 9-30.

Bratby J. Chapter 3. Coagulants. In: *Coagulation and Flocculation in Water and Wastewater Treatment*. London, UK: IWA Publishing, 2006. p. 31-71.

Chalaturnyk RJ, Don Scott J, Özüim B. Management of oil sands tailings. *Petrol Sci Technol* 2002;20(9-10):1025-1046.

Concha A. F. Chapter 1. Introduction. In: Concha A. F, editor. *Solid-Liquid Separation in the Mining Industry*. Cham: Springer International Publishing, 2014. p. 1-10.

Concha A. F. Chapter 7. Particle Aggregation by Coagulation and Flocculation. In: Concha A. F, editor. *Solid-Liquid Separation in the Mining Industry*. Cham: Springer International Publishing, 2014. p. 143-172.

Dragunski D, Pawlicka A. Preparation and characterization of starch grafted with toluene poly (propylene oxide) diisocyanate. *Materials Research* 2001;4(2):77-81.

Environmental Defence Canada (EDC) and Natural Resources Defense Council (NRDC). *One trillion litres of toxic waste and growing: Alberta's tailings ponds*. 2017.

Erbil C, Gökçeören AT, Polat YO. N-isopropylacrylamide–acrylamide copolymers initiated by ceric ammonium nitrate in water. *Polym Int* 2007;56(4):547-556.

Falk H, Stanek M. Two-dimensional ^1H and ^{13}C NMR spectroscopy and the structural aspects of amylose and amylopectin. *Monatshefte für Chemie / Chemical Monthly* 1997;128(8):777-784.

Government of Alberta C. Environmental management of Alberta's oil sands. 2009.

Inoue Y, Fukutomi T, Chujo R. Carbon-13 NMR analysis of the tacticity of polyacrylamide. *Polym J* 1983;15(1):103-105.

Israelachvili JN. Chapter 14. Electrostatic Forces between Surfaces in Liquids. In: *Intermolecular and Surface Forces*. Burlington, MA: Academic Press, 2011. p. 291-340.

Karmakar NC, Rath SK, Sastry BS, Singh RP. Investigation on flocculation characteristics of polysaccharide-based graft copolymers in coal fines suspension. *J Appl Polym Sci* 1998;70(13):2619.

Kennedy JF, Knill CJ, Liu L, Panesar PS. Starch and its Derived Products: Biotechnological and Biomedical Applications. In: *Renewable Resources for Functional Polymers and Biomaterials: Polysaccharides, Proteins and Polyesters*: The Royal Society of Chemistry, 2011. p. 130-165.

Kolya H, Tripathy T. Biodegradable flocculants based on polyacrylamide and poly(N,N-dimethylacrylamide) grafted amylopectin. *Int J Biol Macromol* 2014;70:26-36.

Kolya H, Tripathy T. Grafted polysaccharides based on acrylamide and N, N-dimethylacrylamide: Preparation and investigation of their flocculation performances. *J Appl Polym Sci* 2013;127(4):2786-2795.

Kumar K, Adhikary P, Karmakar N, Gupta S, Singh RP, Krishnamoorthi S. Synthesis, characterization and application of novel cationic and amphoteric flocculants based on amylopectin. *Carbohydr Polym* 2015;127:275-281.

Lee CS, Robinson J, Chong MF. A review on application of flocculants in wastewater treatment. *Process Saf Environ Prot* 2014;92(6):489-508.

Lin-Vien D, Colthup NB, Fateley WG, Grasselli JG. Appendix 3 - A Summary of Characteristic Raman and Infrared Frequencies. In: *The Handbook of Infrared and Raman Characteristic Frequencies of Organic Molecules*. San Diego: Academic Press, 1991. p. 477-490.

Masliyah JH, Xu Z, Czarnecki JA, Dabros M. Chapter 1. Introduction to the Athabasca Oil Sands. In: *Handbook on Theory and Practice of Bitumen Recovery from Athabasca Oil Sands*. Cochrane, Alta.: Kingsley Knowledge Pub., 2011. p. 1-49.

Masliyah JH, Xu Z, Czarnecki JA, Dabros M. Chapter 4. Physical and Chemical Properties of Oil Sands. In: *Handbook on Theory and Practice of Bitumen Recovery from Athabasca Oil Sands*. Cochrane, Alta.: Kingsley Knowledge Pub., 2011. p. 173-266.

Masliyah JH, Xu Z, Czarnecki JA, Dabros M. Chapter 8. Colloidal Science in Tailings Management. In: *Handbook on Theory and Practice of Bitumen Recovery from Athabasca Oil Sands*. Cochrane, Alta.: Kingsley Knowledge Pub., 2011. p. 391-452.

Mino G, Kaizerman S. A new method for the preparation of graft copolymers. Polymerization initiated by ceric ion redox systems. *Journal of Polymer Science Part A: Polymer Chemistry* 1958;31(122):242-243.

Mora-Gutierrez A, Baianu IC. Carbon-13 nuclear magnetic resonance studies of chemically modified waxy maize starch, corn syrups, and maltodextrins. Comparisons with potato starch and potato maltodextrins. *J Agric Food Chem* 1991;39(6):1057-1062.

Olatunji O. Chapter 1. Classification of Natural Polymers. In: *Natural Polymers : Industry Techniques and Applications*. Cham: Springer, 2016. p. 1-17.

Pal S, Pal A. Synthesis and characterizing a novel polymeric flocculant based on amylopectin-graft-polyacrylamide-graft-polyacrylic acid [(AP-g-PAM)-g-PAA]. *Polymer bulletin* 2012;69(5):545-560.

Paris M, Bizot H, Emery J, Buzaré JY, Buléon A. Crystallinity and structuring role of water in native and recrystallized starches by ¹³C CP-MAS NMR spectroscopy. *Carbohydrate Polymers* 1999;39(4):327-339.

Pavia DL, Lampman GM, Kriz GS. Chapter 2. Infrared Spectroscopy. In: *Introduction to Spectroscopy: A Guide for Students of Organic Chemistry*. Fort Worth: Harcourt College Publishers, 2001.

Pavia DL, Lampman GM, Kriz GS. Chapter 3. Nuclear Magnetic Resonance Spectroscopy. Part One: Basic Concepts. In: *Introduction to Spectroscopy: A Guide for Students of Organic Chemistry*. Fort Worth: Harcourt College Publishers, 2001.

Pavia DL, Lampman GM, Kriz GS. Chapter 6. Nuclear Magnetic Resonance Spectroscopy. Part Four: Other Topics in One-Dimensional NMR. In: Introduction to Spectroscopy: A Guide for Students of Organic Chemistry. Fort Worth: Harcourt College Publishers, 2001.

Rath S, Singh R. Grafted amylopectin: applications in flocculation. Colloids Surf Physicochem Eng Aspects 1998;139(2):129-135.

Rath SK, Singh RP. Flocculation characteristics of grafted and ungrafted starch, amylose, and amylopectin. J Appl Polym Sci 1997;66(9):1721-1729.

Rutenberg MW. Starch and Its Modifications. In: Handbook of Water-Soluble Gums and Resins: New York: McGraw-Hill, c1980, 1980. p. 1-6.

Sarkar AK, Mandre N, Panda A, Pal S. Amylopectin grafted with poly (acrylic acid): Development and application of a high performance flocculant. Carbohydr Polym 2013;95(2):753-759.

Sasmal D, Kolya H, Tripathy T. Amylopectin-g-poly(methylacrylate-co-sodium acrylate): An efficient Cd(II) binder. Int J Biol Macromol 2016;91:934-945.

Sasmal D, Singh R, Tripathy T. Synthesis and flocculation characteristics of a novel biodegradable flocculating agent amylopectin-g-poly (acrylamide-co-N-methylacrylamide). Colloids Surf Physicochem Eng Aspects 2015;482:575-584.

Scholz M. Chapter 7. Coagulation and Flocculation. In: Scholz M, editor. Wetlands for Water Pollution Control (Second Edition): Elsevier, 2016. p. 37-46.

Singh RP, Karmakar GP, Rath SK, Karmakar NC, Pandey SR, Tripathy T, Panda J, Kanan K, Jain SK, Lan NT. Biodegradable drag reducing agents and flocculants based on polysaccharides: Materials and applications. *Polym Eng Sci* 2000;40(1):46-60.

Singh RP, Pal S, Rana VK, Ghorai S. Amphoteric amylopectin: A novel polymeric flocculant. *Carbohydr Polym* 2013;91(1):294-299.

Singh V, Kumar P, Sanghi R. Use of microwave irradiation in the grafting modification of the polysaccharides—A review. *Progress in polymer science* 2012;37(2):340-364.

Vedoy DR, Soares JB. Water-soluble polymers for oil sands tailing treatment: A Review. *The Canadian Journal of Chemical Engineering* 2015;93(5):888-904.

Wang J, Yuan S, Wang Y, Yu H. Synthesis, characterization and application of a novel starch-based flocculant with high flocculation and dewatering properties. *Water Res* 2013;47(8):2643-2648.

Williams PA. Chapter 1: Introduction. In: *Handbook of Industrial Water Soluble Polymers*. Oxford ;Ames, Iowa: Blackwell Pub., 2007. p. 1-9.

Williams PA. Chapter 6. Polymeric Flocculants. In: *Handbook of Industrial Water Soluble Polymers*. Oxford ;Ames, Iowa: Blackwell Pub., 2007. p. 134-173.

Appendix A: NTU Calibration Curve

Table A.1. Turbidity of MFT solutions with different solid contents.

Number	Solids content (wt. %)	Turbidity (NTU)
1	37 (Undiluted MFT)	10,000
2	20	10,000
3	15	10,000
4	10	10,000
5	5	10,000
6	4	10,000
7	3	10,000
8	2	10,000
9	1	10,000
10	0.75	10,000
11	0.5	10,000
12	0.25	2670
13	0.2	2182
14	0.1	831
15	0.06	428
16	0.04	268
17	0.02	124
18	0.01	59
19	0.005	32
20	0 (DI water)	0.24

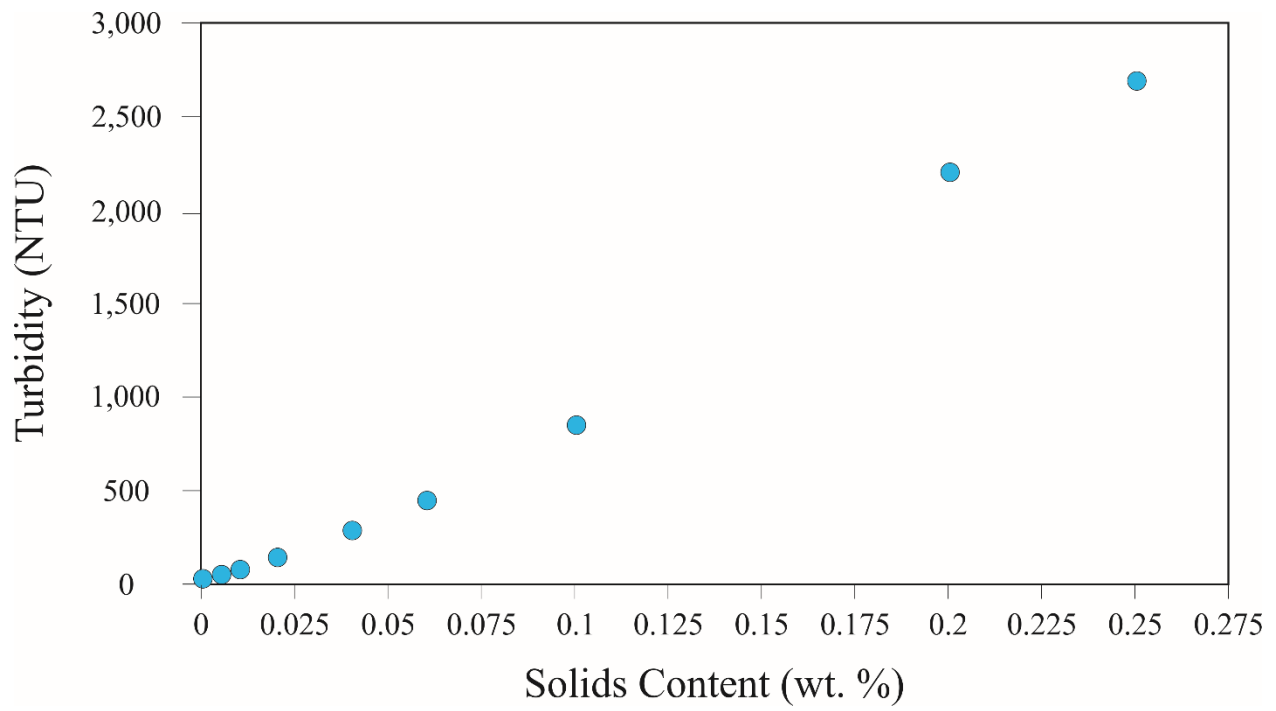


Figure A.1. Turbidity calibration curve: Turbidity (NTU) versus solids content (wt. %) of MFT solutions.



Figure A.2. MFT samples with different solid contents (First number in each picture shows the solid content of MFT suspension (wt. %), and the second one shows the turbidity value in NTU).

Appendix B: Flocculation Results

Table B.1. Flocculation Results (Turbidity and Solids Content).

Polymer	Dosage	Turbidity (NTU)	Error*	Solids Content (wt.%)	Error*
AP	4000	5510	56	30.8	0.1
	6000	2537	7	29.2	0.2
	8000	1746	1	31.5	0.5
	10000	1466	6	28.5	0.4
H-2.5	4000	7940	34	35.4	0.1
	6000	553	4	36.3	0.1
	8000	103	0.5	37.2	0.3
	10000	98	0	30.2	1
AP-H-2.5	4000	10000	0	29.4	1.43
	6000	594	6.7	34.6	0.7
	8000	92	0.4	35.2	0.7
	10000	124	0.3	34.2	0.2
G-4-2.5	4000	3550	4	31.9	1
	6000	264	0.3	32.7	0.2
	8000	175	0.3	35.7	0.2
	10000	406	0.3	35.5	0
H-2.5 ₂	4000	7628	56.9	31.9	0.6
	6000	605	1.7	31	0.1
	8000	90	0.4	31.1	0.4
	10000	127	0.6	29.7	0.7
G-4-2.5 ₂	4000	3353	31.7	23.9	1
	6000	726	5.3	29.4	2.5
	8000	182	0.3	36.3	0.6
	10000	264	1.2	33.8	0.3
G-4-0.25	4000	8776	11.2	26.8	0.8
	6000	967	2	29.6	0.5
	8000	113	0	29.3	0.4
	10000	228	0	28.1	0.2
G-4-0.5	4000	2410	14.3	27.2	0.8
	6000	1438	2.8	26.8	1
	8000	174	0	29.3	0.5
	10000	224	1.8	30.3	0.4
G-4-1.5	4000	485	1.5	20.3	1.7

	6000	222	0.3	32.6	0.5
	8000	354	0.9	30.3	0.3
	10000	387	1.5	31	0.3
G-6-3.5	4000	104	0.6	38.1	0.1
	6000	131	0.6	37.7	1
	8000	147	0.3	34.4	1.4
	10000	122	0.3	38.4	0.7
G-6-2.5	4000	125	0.3	39.9	0.6
	6000	275	1.5	39.5	2
	8000	275	1	33.1	0.9
	10000	182	0.3	35	1.2
G-8-3.5	4000	7335	63.1	39.6	2.2
	6000	1799	7	34.8	1.1
	8000	29	0.2	36.6	0
	10000	131	0	41.7	1.5
G-8-2.5	4000	7170	48.5	26.4	0.4
	6000	2969	6	35.1	0.3
	8000	285	2.6	34	0.1
	10000	143	0	36.6	0.2
G-8-5	4000	3317	7.4	26.9	1
	6000	571	0.6	26.9	0.1
	8000	62	0	29	0.2
	10000	175	0.6	35.5	0.5
CP1	4000	3417	62.5	28.3	0.2
	6000	125	1.5	30.1	0.3
	8000	145	0.3	33.7	0.8
	10000	223	0.9	32.9	0.5
CP2	4000	40	0.4	26.3	2
	6000	58	0.4	31	0.1
	8000	49	0.2	25.2	0.7
	10000	45	0.2	25.9	1.5

*Standard error of the mean

Table B.2. Flocculation Results (CSTs of whole suspension and sediment).

Polymer	Dosage	CST (s)	Error*	CST of Sediment (s)	Error*
AP	4000	113	13	398.3	44
	6000	180.2	28.3	478.6	20
	8000	195.1	18.5	401.2	40.2
	10000	241.4	18.9	401.5	30.5
H-2.5	4000	37.2	10.6	68.6	8.2
	6000	8.8	0.2	93	13.7
	8000	9.2	0.3	116.3	17
	10000	24.9	1.1	76.7	8.3
AP-H-2.5	4000	51.5	7.7	43.9	4.3
	6000	12	1	119.1	16.1
	8000	22.9	1.3	137.7	14.8
	10000	31.2	1.7	104	28.1
G-4-2.5	4000	20	2.5	13	0.1
	6000	7.1	0.2	20	5.2
	8000	7	0.9	102.2	5
	10000	10	0.4	105.7	7.6
H-2.5 ₂	4000	54.3	1.9	72.4	6.9
	6000	12.4	0.3	145.9	7.7
	8000	19.5	1.6	130.9	1.6
	10000	28.7	6.3	113.4	20
G-4-2.5 ₂	4000	32.5	1.2	21.5	2
	6000	16	1.6	28.7	7.4
	8000	14.3	0.5	19.9	1.6
	10000	24.4	2.7	30	4.3
G-4-0.25	4000	48.8	3	72.5	10
	6000	10.6	1.2	33.3	5.6
	8000	5.3	0.1	58.6	7.1
	10000	8.8	0.6	56.2	6
G-4-0.5	4000	58.1	0.8	133.6	7.3
	6000	51.6	1.9	69	5.4
	8000	9.7	0.7	16.9	3.2
	10000	5.2	0.7	69.2	6.2
G-4-1.5	4000	9.6	1.1	20.4	3
	6000	6.9	0.3	35	5.4
	8000	10.3	60.6	54.2	7.6
	10000	10.6	0.8	41.7	9.3
G-6-3.5	4000	7.2	1.1	96.4	13.1
	6000	14.4	2.2	102.7	17.1

	8000	6.3	0.5	143.4	10.7
	10000	10.6	0.6	127.3	12.6
G-6-2.5	4000	8	0.5	215	10.5
	6000	26.6	1.5	250.3	9
	8000	6.9	0.4	234.8	11.2
	10000	8.4	0.4	285	8.4
G-8-3.5	4000	27.2	1.8	108.1	13
	6000	9.5	0.4	98.4	16
	8000	7.4	0.9	198.5	6.3
	10000	9.7	0.1	257	10.3
G-8-2.5	4000	29.5	2	50.9	1.4
	6000	13.3	0.5	55.7	7.5
	8000	6.4	0.3	191.9	15
	10000	14.7	1	170	12.2
G-8-5	4000	19.9	1.6	129	10.2
	6000	9.5	0.7	89.3	4.8
	8000	6.5	0.1	107.9	17.4
	10000	11	0.7	260.2	9.6
CP ₁	4000	47.4	2.8	32	9.3
	6000	11.6	1	43.9	4.1
	8000	10	1	55.6	1.8
	10000	20.2	1.5	74.4	10.9
CP ₂	4000	42.6	3.6	117.6	2.5
	6000	64.6	3.7	120.5	6.4
	8000	95.7	3.7	139.2	16.4
	10000	117.7	11	65.5	4.9

*Error: Standard error of the mean

Table B.3. Sieve tests results at 6,000 ppm.

Polymer	Time (h)	Solids Content (wt. %)	Error*
CP ₁	0	30.8	1
	0.5	36.2	0.4
	1	36.7	0.1
CP ₂	0	15.4	1
	0.5	22.6	0.4
	1	27.9	0.6
G-6-3.5	0	25.2	0.8
	0.5	33.3	0.6
	1	34.1	0.8
G-6-2.5	0	27.8	0.5
	0.5	34.2	0.7
	1	35.6	0.2
G-8-3.5	0	25.3	0.2
	0.5	32.8	0.1
	1	33.1	0.2
G-8-2.5	0	28.4	2.1
	0.5	35.6	0.8
	1	35.9	0.1
G-8-5	0	30.4	1
	0.5	34.5	0.4
	1	37.7	0.3
H-3.5	0	24.9	0.6
	0.5	31.8	1.4
	1	33	1.3
H-5	0	22.7	0.9
	0.5	30.3	0.2
	1	32.7	1

*Error: Standard error of the mean

Table B.4. Sieve tests results at 8,000 ppm.

Polymer	Time (h)	Solids Content (wt. %)	Error*
CP ₁	0	21.5	1.2
	0.5	32.3	0.4
	1	34.8	0.6
CP ₂	0	17	1
	0.5	24.5	0.2
	1	26.8	0.7
G-6-3.5	0	27.8	0.8
	0.5	32.7	0.7
	1	34	1
G-6-2.5	0	22.4	0.1
	0.5	31.8	0.3
	1	32.4	0.2
G-8-3.5	0	21.7	1.6
	0.5	32.1	0.4
	1	34.2	1.6
G-8-2.5	0	28.9	0.1
	0.5	34.7	0.5
	1	35.7	0.2
G-8-5	0	24.9	0.3
	0.5	32.8	0.5
	1	35.1	0.4
H-3.5	0	15.4	1.5
	0.5	27.9	0.8
	1	30.6	0.7
H-5	0	15.9	0.5
	0.5	27.2	0.8
	1	27.9	0.7

*Error: Standard error of the mean

Table B.5. Sieve tests results at 10,000 ppm.

Polymer	Time (h)	Solids Content (wt. %)	Error
CP ₁	0	19.2	1
	0.5	28.3	0.3
	1	31.4	0.6
CP ₂	0	16.3	0.9
	0.5	29.7	0.1
	1	29.8	0.4
G-6-3.5	0	16.9	0.5
	0.5	29.1	0.8
	1	30	0.6
G-6-2.5	0	24.4	0.2
	0.5	34.2	0.7
	1	34.9	0.9
G-8-3.5	0	22.2	0.3
	0.5	29.4	0.9
	1	29.8	0.5
G-8-2.5	0	24.4	0.2
	0.5	30	1.7
	1	30.9	1
G-8-5	0	18.8	0.5
	0.5	28.8	1.2
	1	31.3	0.9
H-3.5	0	21.1	0.4
	0.5	31.4	2.1
	1	33.8	0.1
H-5	0	17.7	0.3
	0.5	27.9	0.4
	1	28.3	1.3

*Error: Standard error of the mean